

Research Article

An evolutionary non-conserved motif in *Helicobacter pylori* arginase mediates positioning of the loop containing the catalytic residue for catalysis

Ankita Dutta¹, Ditsa Sarkar¹, Pooja Murarka¹, Tasneem Kausar¹, Satya Narayan², Mohit Mazumder³, Sri Rama Koti Ainavarapu²,  Samudrala Gourinath³ and  Apurba Kumar Sau¹

¹National Institute of Immunology, Aruna Asaf Ali Marg, New Delhi 110067, India; ²Departments of Chemical Sciences, Tata Institute of Fundamental Research, Dr. Homi Bhabha Road, Colaba, Mumbai 400005, India; ³School of Life Sciences, Jawaharlal Nehru University, New Delhi 110067, India

Correspondence: Apurba Kumar Sau (apurbaksau@gmail.com, apurba@nii.res.in)

The binuclear metalloenzyme *Helicobacter pylori* arginase is important for pathogenesis of the bacterium in the human stomach. Despite conservation of the catalytic residues, this single Trp enzyme has an insertion sequence (–¹⁵³ESEEKAWQKLCSL¹⁶⁵–) that is extremely crucial to function. This sequence contains the critical residues, which are conserved in the homolog of other *Helicobacter* gastric pathogens. However, the underlying basis for the role of this motif in catalytic function is not completely understood. Here, we used biochemical, biophysical and molecular dynamics simulations studies to determine that Glu155 of this stretch interacts with both Lys57 and Ser152. These interactions are essential for positioning of the motif through Trp159, which is located near Glu155 (His122–Trp159–Tyr125 contact is essential to tertiary structural integrity). The individual or double mutation of Lys57 and Ser152 to Ala considerably reduces catalytic activity with Lys57 to Ala being more significant, indicating they are crucial to function. Our data suggest that the Lys57–Glu155–Ser152 interaction influences the positioning of the loop containing the catalytic His133 so that this His can participate in catalysis, thereby providing a mechanistic understanding into the role of this motif in catalytic function. Lys57 was also found only in the arginases of other *Helicobacter* gastric pathogens. Based on the non-conserved motif, we found a new molecule, which specifically inhibits this enzyme. Thus, the present study not only provides a molecular basis into the role of this motif in function, but also offers an opportunity for the design of inhibitors with greater efficacy.

Introduction

Helicobacter pylori (*H. pylori*) is a human gastric pathogen that has infected nearly 50% of the world's population [1]. It causes gastritis and peptic ulcers and predisposes the infected individual to gastric adenocarcinomas [2–5]. Similar to other arginases, the *H. pylori* homolog (encoded by the *rocF* gene) is a bimetallic enzyme that utilizes either Co²⁺ or Mn²⁺ ions for the hydrolysis of host-derived L-arginine into L-ornithine and urea [6–8]. Urea is then hydrolyzed by the bacterial urease to generate ammonia and carbon dioxide. This ammonia is essential for acid resistance in the human stomach and enables the bacteria to colonize near the gastric epithelial layer [9,10]. The bacterial arginase is also known to modulate both the innate and adaptive immunity in the host [11–14]. This helps the bacterium evade the hostile microenvironment and facilitate pathogenesis. Nitric oxide (NO), a mediator of innate immunity is synthesized from L-arginine by the host macrophages using inducible-nitric

Received: 17 December 2020
Revised: 21 January 2021
Accepted: 22 January 2021

Accepted Manuscript online:
22 January 2021
Version of Record published:
24 February 2021

oxide synthase (*i*NOS) to kill pathogens [15]. It was previously reported that NO production in the host macrophages is substantially increased after infection with the *rocF*-deficient *H. pylori* mutant as compared with that of the wild type bacteria [16]. This arginase also inhibits T-cell proliferation by down-regulating the expression of the CD3 ζ chain of the T-cell receptor [14], thereby affecting the adaptive immune response. Thus, these help the bacteria to colonize in the host; and the enzyme is also considered a new virulence factor [17].

Among arginases, the X-ray crystal structure and biochemical function of the human homolog in the absence and presence of various inhibitors have been studied extensively [19–29] and the mechanism of arginine hydrolysis in this homolog has been outlined [21]. In general, this enzyme has three metal-coordinating motifs, namely GGDHS, DxHxD and SxDxDxxDP [29–32]. However, in the *H. pylori* homolog, the GGDHS motif is replaced by SSEHA, though the metal-binding His residue is conserved (Figure 1). These motifs are essential to the formation of a bimetallic center that bridges a water molecule and makes it reactive for the nucleophilic attack on the guanidinium group of L-arginine. It has been suggested that this forms L-ornithine via a tetrahedral intermediate [21]. Although the *H. pylori* enzyme has been reported to exhibit nearly 4-fold higher catalytic activity with Co²⁺ ions as compared with Mn²⁺ [33], the X-ray crystal structure is available only with Mn²⁺ ions [34]. The enzyme has conserved catalytic residues, Asp120, His133 and Glu281 [35] (Figure 1). Asp120 is also found to co-ordinate with the bridging water molecule [34] and has been suggested to further enhance its nucleophilicity. The interaction of His133 with Glu281 has recently been shown to be essential to the catalytic function [35]. It was suggested that this assists in the proton transfer from His133 to the tetrahedral intermediate, which subsequently leads to the formation of L-ornithine (Figure 2) [35]. In the *H. pylori* enzyme, the catalytic His residue is present in a segment (–¹²²HTAYDSDSKHIHG¹³⁴–) that forms a loop. Recently, in the *H. pylori* holoprotein, the divalent metal ions at the metal-binding sites have been shown to modulate the positioning of this loop [35]. This subsequently results in a variation of the distance between His133 and Glu281 in the Co²⁺- and Mn²⁺-reconstituted proteins and explains the difference in their catalytic activity. This is in contrast with the observation of the catalytic activity in the human homolog where the *k*_{cat} value is comparable in the presence of Co²⁺ or Mn²⁺ ions (*k*_{cat} ~ 260 s^{–1}) [18,26,27,36–38]. This suggests that the active site architecture of arginase in these two homologs is modulated differently in the presence of the two different metal ions [35].

We previously reported that *H. pylori* arginase has a non-conserved stretch of 13-residues (–¹⁵³ESEKAWQKLCSL¹⁶⁵–), which is found in the middle of the protein sequence [39] (Figure 1). This stretch forms a helix [34] and is found to be critical to function and stability [39]. We also reported that this stretch is present only in the arginase of *Helicobacter* gastric pathogens, suggesting that this segment might have evolved in a unique manner for a specific function [40]. We showed that three residues — Glu155, Trp159, and Cys163 — belonging to this stretch in the *H. pylori* enzyme were individually crucial to catalytic function and only present in the arginase of *Helicobacter* gastric pathogens [39,40]. Out of these, the role of Trp159 and Cys163 in the *H. pylori* enzyme has been studied [39,40]. It has been shown that Cys163 is crucial to the regulation of activity through the dimerization of the protein [39]. On the other hand, Trp159 interacts with both His122 and Tyr125 and forms an aromatic triad [40]. This was observed only in the *H. pylori* holoprotein through a metal-induced conformational rearrangement, which is vital to optimum catalytic activity. However, the aromatic triad was not observed in the crystal structure of the holoprotein, suggesting that, in solution with the metal ions, the protein adopts a specific conformation with these three aromatic residues. Furthermore, it has been suggested that the formation of this triad occurs by the proper positioning of the non-conserved motif through Trp159. It may be noted that His122 and Tyr125 are also exclusively conserved in the arginase of *Helicobacter* gastric pathogens, including *H. pylori* (Figure 1) [40]. This suggests that these three aromatic residues of arginase belonging to *Helicobacter* gastric pathogens have co-evolved for the enzymatic function. It was previously shown that the mutation of Glu155 to Ala leads to a complete loss of catalytic function [39]. This mutation primarily showed a decrease in helical content (~11% reduction compared with wild type) [39]. These results suggest the role of Glu155 in both the structure and function of the protein. Despite restoration of the secondary structure in this mutant using a known α -helix inducing agent, the Glu155Ala variant showed negligible activity (~2% of wild type), indicating that Glu155 has direct/indirect role in catalytic function [39]. However, the catalytic residues in this enzyme are conserved and their roles have been elucidated [35]. This observation suggests that Glu155 in the non-conserved stretch of arginase may have been selected during the evolution of *H. pylori* in a specific manner to perform its function.

As described, Glu155 and Trp159 of *H. pylori* arginase are located in the same stretch. These two residues are also conserved in the arginase of other *Helicobacter* gastric pathogens. It is possible that, in the *H. pylori*

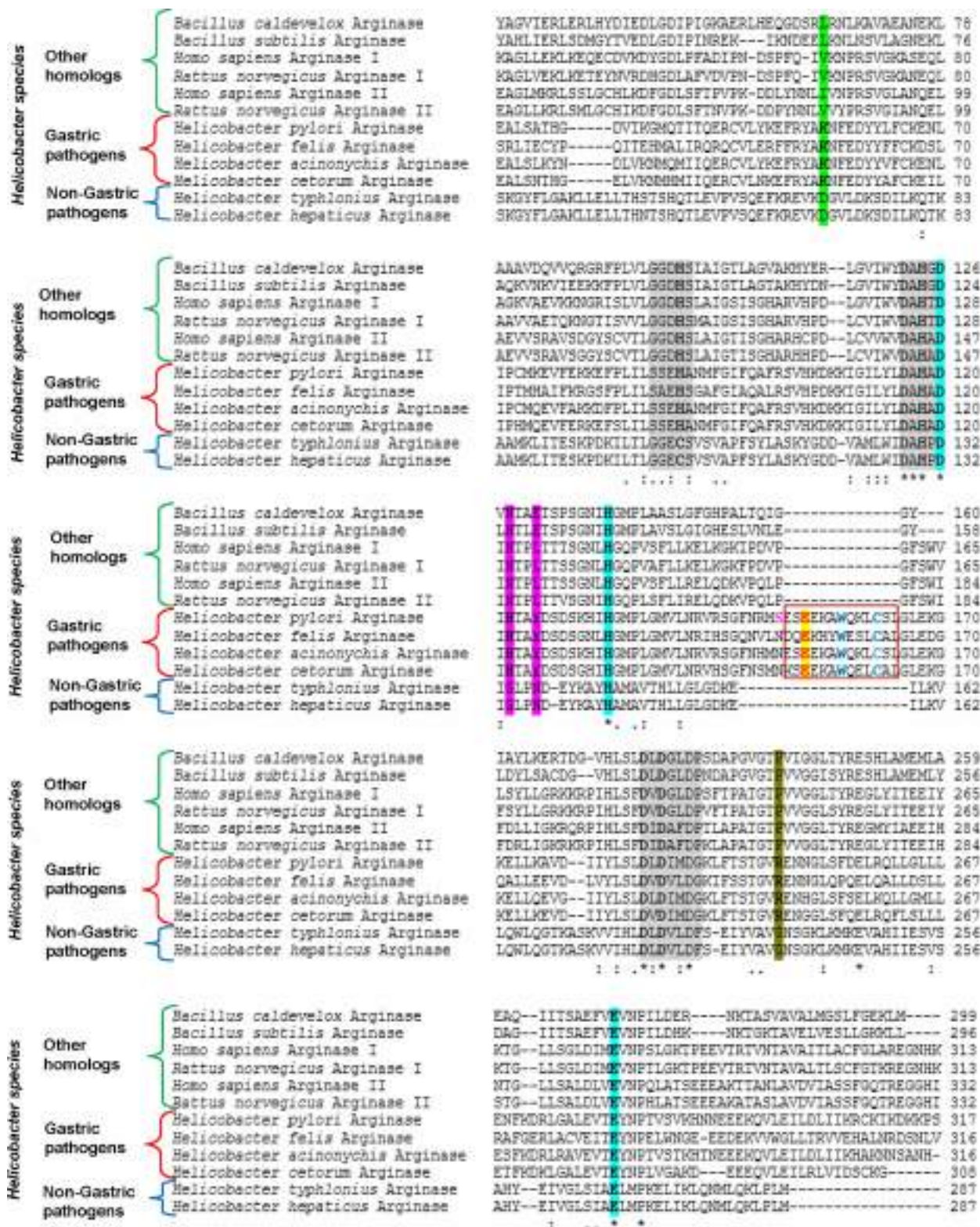


Figure 1. Sequence alignment of arginase belonging to *Helicobacter* gastric and non-gastric pathogens, and other homologs. Part 1 of 2
The signature motifs highlighted in gray color contain the metal-coordinating residues (shown in bold font) enable the formation of a bimetallic center. The conserved catalytic residues of arginases are highlighted in cyan (Asp120, His133 and Glu281 in *H. pylori* arginase). Asp120 is known to be a metal-coordinating residue and important for catalysis [34]. The maroon box shows the insertion motif containing 13-residues (153–165) with

Figure 1. Sequence alignment of arginase belonging to *Helicobacter* gastric and non-gastric pathogens, and other homologs.

Part 2 of 2

Glu155 (red), Trp159 (blue) and Cys163 (blue) being critical. His122 and Tyr125, and their analogous residues are highlighted in magenta, which are found only in the arginase of *Helicobacter* gastric pathogens. They form aromatic contacts with Trp159 through positioning of the insertion motif. The Lys57 residue of the *H. pylori* enzyme is shown in bold font and highlighted along with its analogous residues in light green color. Ser152 of *H. pylori* arginase is shown in pink color. Arg249 and its analogous residues are highlighted in golden color and this residue is not conserved in the homologs of *H. pylori* arginase. The N- and C-terminal residues are excluded for clarity.

enzyme, besides Trp159, Glu155 may influence the positioning of this motif through its specific interactions with residue(s) and, thus, in the catalytic function. To explore this and investigate its underlying mechanism, we have undertaken a combination of approaches that include mutational analysis, kinetic assays, circular dichroism, heat-induced denaturation, anisotropy decay kinetics, and molecular dynamics (MD) simulations. We used *H. pylori* arginase for this study because, among *Helicobacter* gastric pathogens, *H. pylori* shows the highest incidence of infection [41]. Our study reveals that Glu155 plays a role in the positioning of the non-conserved stretch through its interactions with both Lys57 and Ser152. Lys57 is conserved in the arginase of other *Helicobacter* gastric pathogens. The study further shows that the interactions involving Lys57–Glu155–Ser152 are crucial to catalytic function, where the interaction with Lys57 has a greater role, highlighting the importance of a new set of non-catalytic residues in catalysis. Our data indicate that these interactions influence the orientation of the catalytic loop which is essential for catalysis. Thus, this study provides a mechanistic insight into the role of this motif in catalytic function. This knowledge has also provided a basis to identify a new molecule that specifically inhibits the *H. pylori* enzyme.

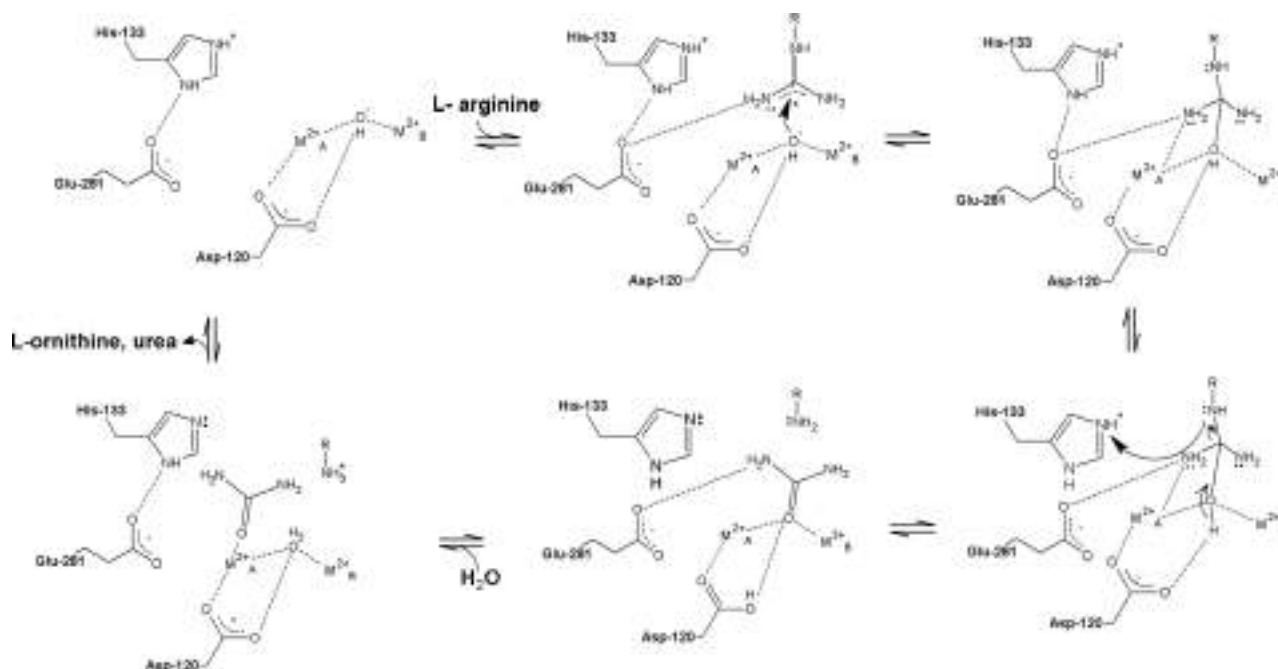


Figure 2. A proposed mechanism of L-arginine hydrolysis by *H. pylori* arginase on the basis of mechanism suggested for human arginase I. For clarity, the active site containing three residues, His133, Asp120 and Glu281, and the two metal ions (M_A^{2+} and M_B^{2+}) are depicted [21]. The metal ions can be either Co^{2+} or Mn^{2+} . A metal bridging water molecule is involved in the nucleophilic attack on the guanidinium carbon of L-arginine, leading to the formation of a tetrahedral intermediate. The proton transfer from the catalytic His133 and subsequent steps involved in the hydrolysis with regeneration of the enzyme are described.

Materials and methods

Mutagenesis

Lys57Ala, Lys57Arg, Lys57Glu, Glu155Lys, Glu155Asp, Arg249Ala, Ser152Ala, Lys57Glu/Glu155Lys and Lys57Ala/Ser152Ala mutants of *H. pylori* arginase were prepared using HF-phusion polymerase (Thermo) and *Pfu* turbo (Agilent Technologies, Glostrup, Denmark) as per the manufacturers' protocol. Appropriate forward and reverse primers mentioned (Supplementary Table S1) were used for polymerase chain reactions using the wild type GST-tagged pC6-2-rocF plasmid already available as template. Positive mutants were identified by DNA sequencing.

Expression and purification of proteins

Expression of the recombinant GST-tag *H. pylori* wild type and mutant proteins was carried out using *Escherichia coli* BL21 (DE3) pLysS-competent cells and their purification was performed using a previously reported protocol with a few modifications [6]. The GST-tag with a caspase-6 cleavage site was removed from the wild type and mutant proteins using the recombinant (His)₆-tagged Caspase-6 following a procedure reported earlier [42]. The eluted protein was mixed with 1 ml of Ni-NTA agarose (Qiagen, CA) column pre-equilibrated with 1X PBS to remove caspase-6 and to obtain the tag-free arginase. The protein sample was again concentrated in a centricon-10 (Millipore, MA, U.S.A.) at 4°C and applied onto a Superdex-200 column, which was pre-equilibrated with 1× PBS (pH 7.4). The fractions were collected, concentrated and stored at –80°C with 10% glycerol. Protein concentrations were estimated spectrophotometrically using the Bradford assay. The tag-free wild type and mutant apoproteins were used for biophysical experiments, metal analysis and kinetic assays.

Human arginase I (hArg-I) was purified following a reported procedure [27].

Activity assay

The activity assay for the Co²⁺-reconstituted wild type and mutant *H. pylori* proteins was carried out spectrophotometrically following a reported procedure [6]. The preparation of the Co²⁺-protein was done by incubating the apoprotein with Co²⁺ ions at a ratio of 1 : 100. The assay was performed at 37°C with 50 mM Tris–HCl, pH 7.4 using 1 μM holoprotein and 20 mM L-arginine. Ornithine formation was monitored at 515 nm with ninhydrin. The holoprotein concentration for all experiments was kept at 1 μM unless mentioned otherwise. Activity assay of hArg-I was performed as reported earlier [27].

For the inhibition study of *H. pylori* and human arginases, the holoenzymes were separately incubated with the inhibitors for 1 h at 37°C and the reaction was initiated as previously described. The percentage of activity was calculated comparing the activity of the enzyme in the absence of the putative inhibitors. For estimation of the IC₅₀ value, a fixed amount of the *H. pylori* holoenzyme was incubated with varying inhibitor concentrations at a particular concentration of the substrate. The plot of percentage of activity vs the inhibitor concentrations was used to determine the IC₅₀ value.

Determination of the metal stoichiometry

For the estimation of metal stoichiometry, the Co²⁺-reconstituted protein was passed through a Sephadex G-25 column equilibrated with 50 mM Tris–HCl, pH 7.4 to remove excess metal ions. The protein in the flow through was concentrated using a centricon-10. The concentration of the protein was estimated by the Bradford assay. A reported protocol with 4-(2-pyridylazo) resorcinol (PAR) dye was used to estimate the stoichiometry of metal ions bound to 1 μM protein [33,39,40,43]. The Co²⁺-reconstituted protein was denatured with 6 M guanidine hydrochloride for 60 min at room temperature. After the addition of PAR to the sample for 20 min, the absorbance was measured at 515 nm for Co²⁺ ions. A standard curve was used to estimate the concentration of the bound metal ions.

Circular dichroism measurement and heat-induced denaturation

Circular dichroism (CD) spectra of the apo- and Co²⁺-reconstituted wild type and mutant proteins in the far-UV range were recorded on a spectropolarimeter (Chirascan, Applied PhotoPhysics, Leatherhead, U.K.) using a cuvette of 1 mm path length in 20 mM Tris–HCl, pH 7.4 at 25°C. The spectra were corrected for their baselines by subtracting the buffer and buffer with metal ions. The *T_m* value of the samples was determined by heating the sample from 25°C to 90°C using a Peltier thermostat coupled with spectropolarimeter at the rate of

1°C/min. The data were recorded at intervals of 1°. For determination of the melting temperature, the normalized θ_{MRW} values at 222 nm were plotted against temperature. The data were fitted using a two-state unfolding model and the reversibility was checked by denaturing the protein at a temperature higher than the T_m value and then cooling it down to room temperature followed by reheating. A similar denaturation profile and T_m were obtained, indicating that heat-induced unfolding occurs in a reversible manner.

Steady-state fluorescence studies

Intrinsic tryptophan fluorescence of the protein was carried out on a Fluoromax 4 (HORIBA Jobin Yvon, Kyoto, Japan) spectrofluorimeter with an excitation wavelength of 295 nm. The emission spectra were recorded from 310 nm to 450 nm. The slit width for all experiments was 3 nm. All measurements were carried out in 50 mM Tris, pH 7.4 at room temperature.

Fluorescence anisotropy decay kinetics

A previously reported procedure using a time-correlated single photon counting setup was implemented to perform the time-resolved fluorescence decay experiments [44,45]. For excitation source, we used a rhodamine 6G dye laser (Spectra Physics, Mountain View, CA), which is pumped by a passively mode-locked, frequency-doubled, neodymium-doped yttrium aluminum garnet laser (Vanguard, Spectra Physics). A frequency doubler (Spectra Physics) was used to double the frequency of the pulses of 590 nm radiation with 1 ps duration from the laser to 295 nm. The instrument response factor (IRF) was measured exciting a diluted colloidal solution of dried non-fat dairy coffee whitener at 295 nm, followed by collecting the emission at the same wavelength with the emission polarizer oriented at 54.7° with respect to the excitation polarizer and is popularly referred to as the ‘magic angle’. The laser full width half-maximum (FWHM) IRF was nearly 40 ps. For the measurements, 20 μ M protein concentration was used and the sample was excited at 295 nm at a pulse repetition rate of 4 MHz. The emission was then collected at 330 nm using a cut-off filter and a monochromator. Furthermore, only decays with peak counts of 10 000 were collected with the emission polarizer oriented at magic-angle (54.7°) with respect to the excitation polarizer. These decay curves were then deconvoluted with respect to IRF and further analyzed to obtain the decay parameters. For the anisotropy decay measurements, the decays for the same sample was collected up to 10 000 peak counts with the emission polarizer kept at parallel ($I_{||}$) and perpendicular (I_{\perp}) orientations with respect to the excitation polarizer using the same experimental setup as described earlier. All these anisotropy decays were also deconvoluted with respect to the IRF.

Data analysis for the fluorescence decay measurements

The fluorescence intensity decays were analyzed by fitting the data to a nonlinear least-squares iterative fitting method based on the Levenberg-Marquardt algorithm [46]. The chi-square (χ^2) values (1–1.5) and the random residual distribution analysis both were synergistically used to evaluate the goodness of the fit. The time-resolved fluorescence intensity decays were found to fit best to a sum of three-exponential functions and were expressed as follows:

$$I(t) = \sum \alpha_i \exp(-t/\tau_i) \quad i = 3, \quad (1)$$

Where $I(t)$ is the fluorescence intensity collected with the emission polarizer oriented at the magic angle (54.7°) with respect to the excitation polarizer at time t and α_i is the amplitude associated with the fluorescence lifetime τ_i , such that $\sum \alpha_i = 1$. Furthermore, the mean fluorescence lifetime was calculated as

$$\tau_m = \sum \alpha_i \tau_i. \quad (2)$$

The lifetime analysis was used to further analyze the anisotropy decay data using a method described earlier [44]. Anisotropy was calculated as follows,

$$r(t) = (I_{||}(t) - G(\lambda)I_{\perp}(t)) / (I_{||}(t) + 2G(\lambda)I_{\perp}(t)),$$

where $I_{||}$ and I_{\perp} are the decays of the parallel ($||$) and perpendicular (\perp) components of emission. $G(\lambda)$ is the

geometry factor at the emission wavelength (λ) and $r(t)$ is the time-dependent anisotropy. The value of the G-factor was calculated independently using a standard solution of N-acetyltryptophanamide (NATA). We then used the following model for the analysis of the time-resolved anisotropy decay:

$$I(t) = I(0)[1 + 2r(t)]/3 \quad (3)$$

$$I(t) = I(0)[1 - r(t)]/3 \quad (4)$$

The equation for time-resolved fluorescence anisotropy can be expressed as a biexponential decay:

$$r(t) = r_0 \sum \beta_i \exp(-t/\phi_i), \quad i = 2, \quad (5)$$

where ϕ_i and β_i represent the i th rotational correlation time and the corresponding pre-exponential factor in the exponential anisotropy decay such that $\sum \beta_i = 1$. r_0 , here presents the anisotropy in the absence of any rotational diffusion. The r_0 value of 0.3 was determined through an independent experiment using the wild type arginase with 70% glycerol. The values for the two rotational correlational times (ϕ_1 and ϕ_2) and their associated amplitudes (β_1 and β_2 , respectively) were derived from fits of the fluorescence anisotropy decays using the above equations. The goodness of the fit was evaluated using both the lower χ^2 values (nearly 1) and random residual distribution.

Molecular docking and virtual screening

To search small-molecule inhibitor from ZINC database, we performed molecular docking based virtual screening using AutoDock 4.2.6 [47] and PyRx software [48]. The simulated structure of *H. pylori* arginase (1.2 microsecond) was used as a macromolecule. We have taken randomly a molecule having at least one or more heteroatom (N, O, S or halogens) from 300 molecular scaffolds each and performed molecular docking with *H. pylori* arginase using AutoDock 4.2.6 software. The protein was kept rigid in a grid box of size $126 \times 126 \times 126$ with grid spacing 0.730, while ligand was allowed to move in the grid box. Two scaffolds were selected for virtual screening based on the lowest binding energy at the desired binding site. The molecular library of these two scaffolds that are ~0.21 million molecules is used for virtual screening using PyRx software in which AutoDock Vina [49] is implemented. During virtual screening, the enzyme was placed in the grid box of the size $50 \times 50 \times 50$ with 0.375 grid spacing. Molecules having binding energy lower than -6.0 kcal/mol and binding to the desired site are selected and further docked with the AutoDock 4.2.6 software.

Molecular dynamics simulations of *H. pylori* arginase

Wild type protein and its mutants

To understand the structural variations in the Lys57Ala, Ser152Ala and Glu155Ala mutants compared with the wild type, the model structure for the wild type *H. pylori* Co^{2+} -arginase was built using the method reported in detail earlier using the crystal structure of *H. pylori* Mn^{2+} -arginase (PDB ID 4G3H) as a template and then superimposing the *H. pylori* arginase structure onto the crystal structure of human Co^{2+} -arginase (PDB ID 3TH7) to obtain the coordinates of the Co^{2+} ions [35]. Then 1.2 μs simulation of the wild type Co^{2+} -arginase was carried out as previously reported [35]. This energy minimized structure was used to generate the *in-silico* mutants Lys57Ala, Ser152Ala and Glu155Ala. These were individually modeled using ROSETTABACKRUB point mutation server and were sampled by Monte Carlo simulated annealing using the Rosetta all-atom force field [50]. After the lowest weighted scored structure was obtained, the hydrogen atoms were added using the *tleap* tool of AMBER14 [51]. The SANDER and PMEMD module of the AMBER14 package with ff14SB force field was used for the MD simulations. The production phase of the simulations was run without any restraints for a total of 100 ns on each system. The analysis of the MD simulations including root-mean-square deviation (RMSD), root-mean-square fluctuations (RMSF) and solvent accessible surface area (SASA) calculations was carried out using the PTRAJ program. The 3D molecular graphics were displayed using PyMol software [52]. This system was then solvated using atomistic TIP3P water in a box with edges at least 12 Å from the protein followed by electrostatic neutralization by addition of Cl^- ions. Energy minimization was first conducted by the steepest descent method and then switched to conjugate gradient every 500 steps for a total of 5000 steps with $0.1 \text{ kcal/mol}/\text{\AA}^2$ restraints on the protein molecule. Long-range columbic interactions were handled using the

particle mesh Ewald summation [53]. For equilibration and subsequent production runs, the SHAKE algorithm was employed on all atoms covalently bonded to a hydrogen atom, which allowed an integration time step of 2 fs. The system was gently annealed for a period of 50 ps using a Langevin thermostat with a coupling coefficient of 1.0 ps^{-1} and 500 ps of density equilibration with weak restraints on the protein molecule. The system was again equilibrated for 1 ns without any restraints. The production phase of the simulations was run without any restraints for a total of 100 ns on each system. The coordinates and energy values were collected every 10 ps throughout the simulations. The data were analyzed using PyMol and Chimera.

Wild type protein with inhibitor

Molecular dynamics simulations of *H. pylori* Co^{2+} -arginase with C3 compound were performed using Gromacs-5.1.4 software [54,55]. The lowest energy structure of the enzyme-inhibitor complex obtained from molecular docking was taken as a starting structure for MD simulations. General Amber force field (GAFF) [56] and AM1-BCC charge method [57] implemented in AmberTools18 [58] was used for the generation of inhibitor topology parameters. Charge and non-bonded parameters for Cobalt (Co^{2+}) were taken from previous report [35]. The topology parameters of the protein were obtained in AMBER99SB-ILDN force field format [59]. The enzyme-inhibitor complex was solvated in a triclinic box with explicit water molecules using periodic boundary conditions. The system was neutralized with the addition of Na^+ ions and subjected to energy minimization using steepest decent method with 2000 steps down to a maximum gradient of $1000 \text{ kJ}^{-1} \text{ mol}^{-1} \text{ nm}^{-1}$. NVT and NPT equilibrations were done for 100 ps. Finally, 200 ns standard MD simulations with NPT ensemble were performed at 300 K temperature. Rest of the MD parameters used in this study were taken from previous study [60]. The MD snapshots were collected at the interval of 10 ps and analyzed by Gromacs utility programs.

Results

Investigation of possible residues that interact with Glu155

To explore the possibility of Glu155 in the positioning of the non-conserved motif through its specific interactions, it was first essential to investigate the residue(s) that interact(s) with Glu155. For this, we initially used the reported 450 ns simulated structure of *H. pylori* apoarginase, as this provided useful structural information, where Trp159 was in close contact with both His122 and Tyr125 [39]. In this structure, we found the presence of only Arg249 whose side chain is nearly 5.6 \AA away from the carboxylate group of Glu155 (Figure 3A). In holoarginases, the metal ions have been shown to induce a conformational rearrangement near the active site, which is essential for catalytic function [40]. Possibly, the above distance between the side chains of these two residues in the *H. pylori* holoprotein might be reduced so that they can make an important contact. To test this and explore whether it plays a role in catalytic function, we prepared an Arg249Ala mutant. The wild type protein was also prepared for comparison. The steady-state kinetic assay of these two proteins was performed in the presence of Co^{2+} -ions, since *H. pylori* Co^{2+} -reconstituted arginase exhibits nearly 4-fold higher catalytic activity as compared with its Mn^{2+} -enzyme. Thus, the subsequent studies reported here were performed only with the Co^{2+} -reconstituted protein. Similar to the earlier reports [39,61], the data for the wild type and mutant proteins were fitted to a sigmoidal equation for purposes of determining the kinetic parameters, k_{cat} (catalytic constant), $K_{0.5}$ (apparent substrate binding affinity for the enzyme), and n (degree of cooperativity) (Supplementary Figure S1). The $k_{\text{cat}}/K_{0.5}$ (apparent catalytic efficiency) values for the wild type and mutant proteins were comparable without individually affecting the magnitude of k_{cat} and $K_{0.5}$ (Table 1, Figure 3B). Moreover, the secondary structure and tryptophan fluorescence emission maxima of the mutant protein (single tryptophan containing *H. pylori* arginase) were similar to those of wild type (data not shown). These observations suggest either that Glu155 does not make contact with Arg249 or that this contact plays no role in catalytic function.

Glu155 interacts with Ser152 and plays a role in catalytic function

To further explore the role of Glu155, the crystal structure of *H. pylori* Mn^{2+} -arginase was examined. Structural analysis revealed that the carboxylate group of Glu155 makes contact only with the side chain hydroxyl of Ser152 and forms an H-bond with a distance of 3.2 \AA (Figure 3C). However, the role of this contact in catalytic function has not been studied. To examine this, a Ser152Ala mutant was prepared and its steady-state kinetic assay was performed. The data were similarly analyzed (Supplementary Figure S1). The catalytic efficiency for

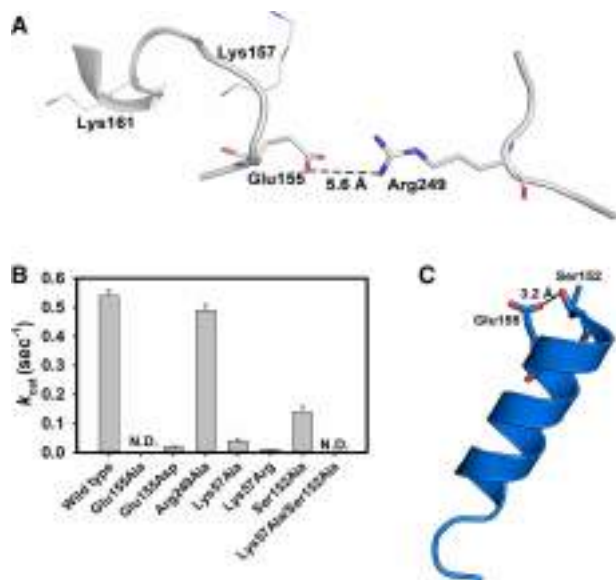


Figure 3. Structural and functional analyses of residues interacting with Glu155 in *H. pylori* arginase. (A) 450 ns simulated structure of *H. pylori* apoarginase reveals that Arg249 is the only positively charged residue present in the proximity of Glu155. Lys157 and Lys161 are part of the insertion motif, but they do not interact with Glu155. (B) The catalytic constant k_{cat} of the wild type *H. pylori* arginase and its mutants are shown. The kinetic assay was performed with a reaction mixture containing 1 μ M apoenzyme and 100 μ M Co^{2+} ions (this ratio of the apoprotein to the metal ion showed optimal catalytic activity) with varying concentrations of L-arginine. The data were analyzed using a previously reported Hill equation, $\text{rate} = k_{cat} \times [\text{E}_0] \times [\text{Arg}]^n / (K_{0.5}^n + [\text{Arg}]^n)$ and the kinetic parameters namely, $K_{0.5}$, k_{cat} and n (Hill coefficient) were estimated. The quality of the fit was determined using a theoretical line drawn through the experimental data points. The assays for the mutants were similarly performed and analyzed. N.D. represents no detectable activity. 0.05% of wild type activity or below was considered to be no activity observed. The values represented here are the average \pm SEM of three independent measurements. (C) The carboxylate group of Glu155 and the hydroxyl side chain of Ser152 were found to interact at a distance of 3.2 Å in the crystal structure of *H. pylori* Mn^{2+} -arginase (PDB 4G3H).

Table 1 Steady-state kinetic parameters for the *H. pylori* wild type and mutant Co^{2+} -arginases

Protein	k_{cat} (sec ⁻¹)	$K_{0.5}$ (mM)	n	$k_{cat}/K_{0.5}$ (sec ⁻¹ mM ⁻¹)
Wild type	0.54 ± 0.02	3.5 ± 0.2	2.2 ± 0.3	0.15
Glu155Ala	N.D.	N.D.	N.D.	N.D.
Glu155Asp	0.02 ± 0.003	2.8 ± 1	1.0 ± 0.3	0.007
Arg249Ala	0.49 ± 0.02	2.9 ± 0.2	2.2 ± 0.4	0.17
Lys57Ala	0.04 ± 0.01	3.5 ± 1.4	1.2 ± 0.4	0.01
Lys57Arg	0.01 ± 0.002	3.9 ± 1.4	1.0 ± 0.2	0.002
Ser152Ala	0.14 ± 0.02	3.5 ± 1.3	1.2 ± 0.4	0.04
Lys57Ala/Ser152Ala	N.D.	N.D.	N.D.	N.D.

Note: N.D. — no detectable activity; 0.05% of wild type activity or below was considered to be ‘no activity observed’. An amount of 1 μ M apoprotein was used for all experiments. The protein was reconstituted with 100 μ M Co^{2+} ions. The ratio of 100 : 1 concentration for Co^{2+} ions and the apoprotein was used to perform the kinetic assays. All data were analyzed using a Hill equation, $\text{rate} = k_{cat} \times [\text{E}_0] \times [\text{Arg}]^n / (K_{0.5}^n + [\text{Arg}]^n)$ and the kinetic parameters apparent $K_{0.5}$, k_{cat} , and n (Hill co-efficient) were determined. A theoretical line drawn through the experimental data points considering the highest confidence limits was used to determine the quality of the fit. All assays were performed with tag free proteins. The values represented here are the average \pm SEM of three independent measurements.

the Ser152Ala mutant was reduced by 4.3-fold compared with that of wild type, where the k_{cat} value was primarily affected without altering the magnitude of $K_{0.5}$ (26% of wild type activity) (Figure 3B, Table 1). This result suggests that the interaction of Glu155 with Ser152 plays a role in catalytic function. As reported, the mutation of Glu155 to Ala leads to a complete loss of catalytic activity [39]. If Glu155 makes contact only with Ser152, one may anticipate a complete loss of catalytic activity in the Ser152Ala mutant, similar to that found for the Glu155Ala variant. However, the observation of 26% of wild type activity in the Ser152Ala mutant suggests that Glu155 may also interact with other residue(s). Thus, the crystal structure of the *H. pylori* Mn^{2+} -protein cannot fully explain the role of Glu155 in catalytic function.

Simulated holoprotein structure reveals an additional interaction of Glu155 with Lys57

To explore whether Glu155 may also interact with other residue(s), efforts were made to crystallize the *H. pylori* Co^{2+} -enzyme and to determine its three-dimensional structure because this exhibits higher catalytic activity than that of the Mn^{2+} -enzyme. Although several crystals were obtained, we could collect only low diffraction data sets. Hence, we could not determine the structure. Instead, we analyzed the recently reported 1.2 μs simulated structures of *H. pylori* Mn^{2+} - or Co^{2+} -arginases because these structures could explain the variation in their catalytic activity [35]. Moreover, the metal-induced conformational rearrangement near the active site of the *H. pylori* protein has been found to be important in the generation of a catalytically competent conformation [40]. For purposes of obtaining the simulated structure of *H. pylori* Mn^{2+} -arginase, its crystal structure was used as a template. However, for the *H. pylori* Co^{2+} -enzyme, its model structure was first generated using the crystal structure of *H. pylori* Mn^{2+} -arginase, where the coordinates of Co^{2+} ions were taken from the reported structure of human Co^{2+} -arginase. In both the Co^{2+} - and Mn^{2+} -simulated structures, Glu155 was found to make contact with Ser152 through its side chain from the beginning of simulations; it remained intact during the simulations (Figure 4A,B). It may be noted that the distance between the side chains of these two residues in the 1.2 μs simulated structure of the Mn^{2+} -protein is decreased compared with that in the crystal structure (3.2 vs 2.5 Å in the crystal structure vs simulated structure, respectively). This observation not only supports stable contact between Glu155 and Ser152 in the simulated structure but also suggests a structural modulation during simulations. In the simulated structure of the Co^{2+} -protein, these two residues also form a stable contact (2.8 Å). Analysis reveals another interesting observation. The carboxylate group of Glu155 makes additional contact with the side chain of Lys57 in both the Co^{2+} - and Mn^{2+} -proteins. For purposes of checking it furthermore, the distance between the side chains of Glu155 and Lys57 was examined from the beginning of the simulations (Figure 4C–F). It is interesting to note that in the Co^{2+} - and Mn^{2+} -proteins, this distance decreased after 160 and 190 ns, respectively. In the Co^{2+} -protein, this distance did not vary during the remaining simulations (Figure 4C,E). However, in the Mn^{2+} -protein, it gradually decreased until 400 ns and then remained almost similar during the rest of the simulations (Figure 4D,F). Additionally, in the simulated structure of the Mn^{2+} -protein, Lys57 was found in a distorted helix (Figure 5A), whereas in the Co^{2+} -protein structure this residue was present in a small loop located between the two helices (shorter and longer helices, Figure 5B). The variation in the structure of the Lys57-containing region in these two holoproteins was observed from the beginning of the simulations and remained throughout. This could be because of the difference in the metal-induced structure of these two holoproteins. Despite this structural difference in the helical region, Lys57 was repositioned during the simulations and became closer to Glu155 in both holoproteins. It is to be noted that the positioning of Glu155 in the insertion motif did not almost vary. This observation suggests that the contact between Glu155 and Lys57 is compelling and may play a role in catalytic function. Additionally, Ser152 was found in a similar position throughout the simulations in both holoproteins.

Glu155–Lys57 interaction is crucial to catalytic function

To examine whether the contact between Glu155 and Lys57 plays a role in catalytic function, we prepared a Lys57Ala mutant. Similar kinetic assay of this mutant was performed and the data were analyzed (Supplementary Figure S1). Interestingly, the catalytic efficiency of the Lys57Ala mutant decreased 16-fold compared with that of wild type, in which the k_{cat} value was decreased without affecting the magnitude of $K_{0.5}$ (6% of wild type activity, Figure 3B, Table 1). This result indicates that the mutation of Lys to Ala at position 57 significantly reduces the catalytic activity. For purposes of assessing the effect of both Lys57 and Ser152 in catalytic function, a double mutant Lys57Ala/Ser152Ala was prepared. As expected, this mutant did not exhibit

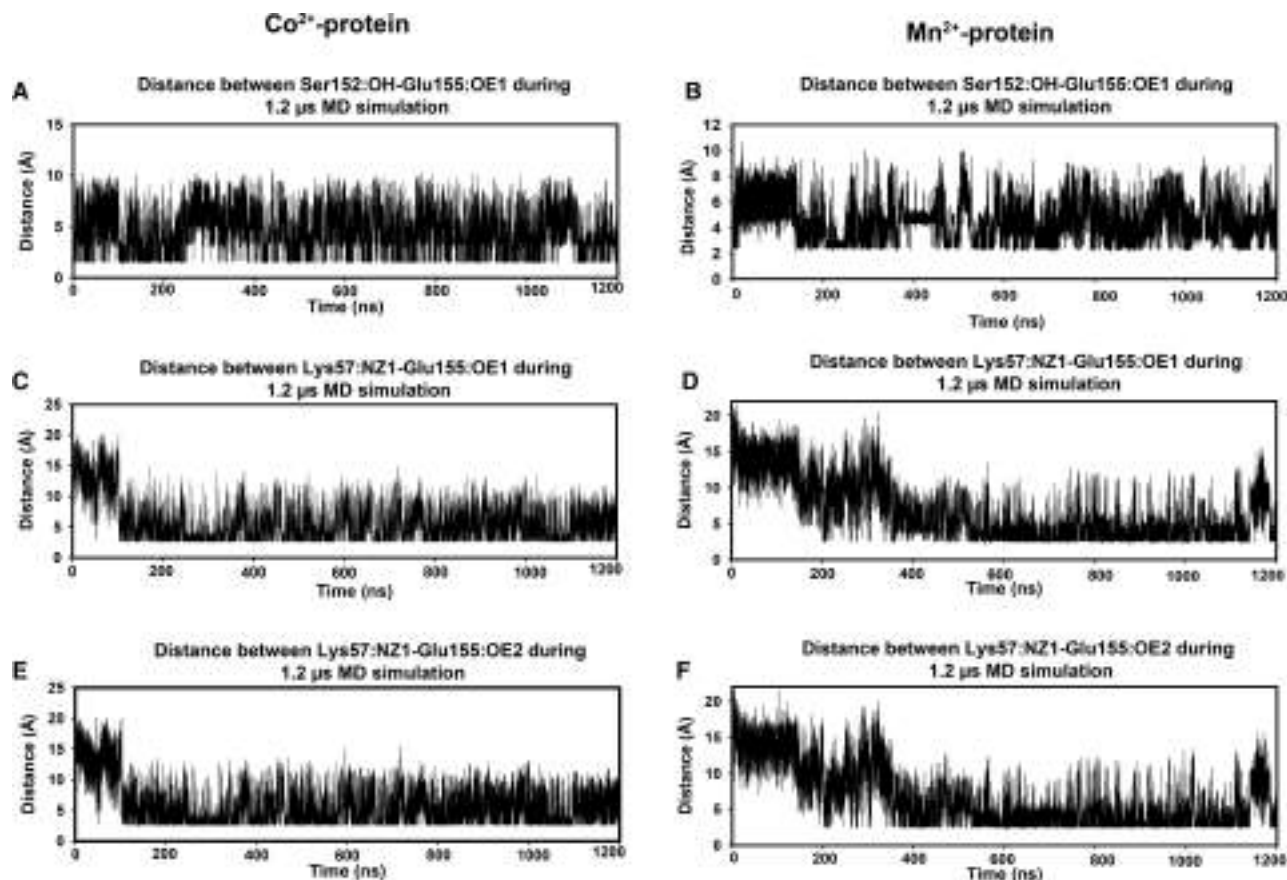


Figure 4. Distance between the residues those interact with Glu155 in *H. pylori* arginase during the course of simulations.

The distance between (A) The Ser152:OH group and the Glu155:OE1 atom in the Co²⁺-protein and (B) in the Mn²⁺- protein is shown during MD simulations. This distance fluctuates throughout the trajectory; however, it decreases to a length where these two residues could possibly interact to form a bond towards the end of simulation. (C) The distance between the Lys57:NZ1 atom and the Glu155:OE1 atom in the Co²⁺-protein decreases with time to a length where these two residues could possibly interact and remains unaltered throughout the rest of the trajectory after 160 ns. (D) The distance between the Lys57:NZ1 atom and the Glu155:OE1 atom in the in Mn²⁺- protein decreases with time to a length where these two residues could possibly interact and remains unaltered throughout the trajectory after 190 ns. (E) the Lys57:NZ1 atom and the Glu155:OE2 atom in the Co²⁺-protein is shown during the time course of MD simulation. (F) The Lys57:NZ1 atom and the Glu155:OE2 atom in the Mn²⁺-protein is shown during the time course of MD simulation.

detectable activity, even with a substrate concentration nearly 6-fold higher than the K_M value of the wild type protein. This result clearly suggests that the interactions of both Lys57 and Ser152 with Glu155 play a crucial role in catalytic function. However, the interaction with Lys57 has a greater role compared with that with Ser152. This may be because of stronger electrostatic interaction between the two oppositely charged Lys57 and Glu155 residues compared with the interaction between the polar residue Ser152 and the negatively charged Glu155.

The biochemical data presented thus far suggest that the interaction of Glu155 with Lys57 plays a critical role in catalytic function. To validate this furthermore, we prepared another two mutants, Glu155Asp and Lys57Arg. In the Glu155Asp mutant, the length of the Glu side chain at position 155 was decreased compared with that of wild type, while that of the Lys side chain at position 57 in the Lys57Arg variant was increased. However, a similar charge was retained in both of these mutants. The kinetic assays of these two single mutants showed a dramatic decrease in catalytic efficiency as compared with wild type, where the k_{cat} value for the Glu155Asp and Lys57Arg mutants was reduced by 30- and 54-fold, respectively without affecting the magnitude of $K_{0.5}$ (3.3% and 1.8% of wild type activity, respectively) (Table 1). The Lys57Arg mutant exhibits lower

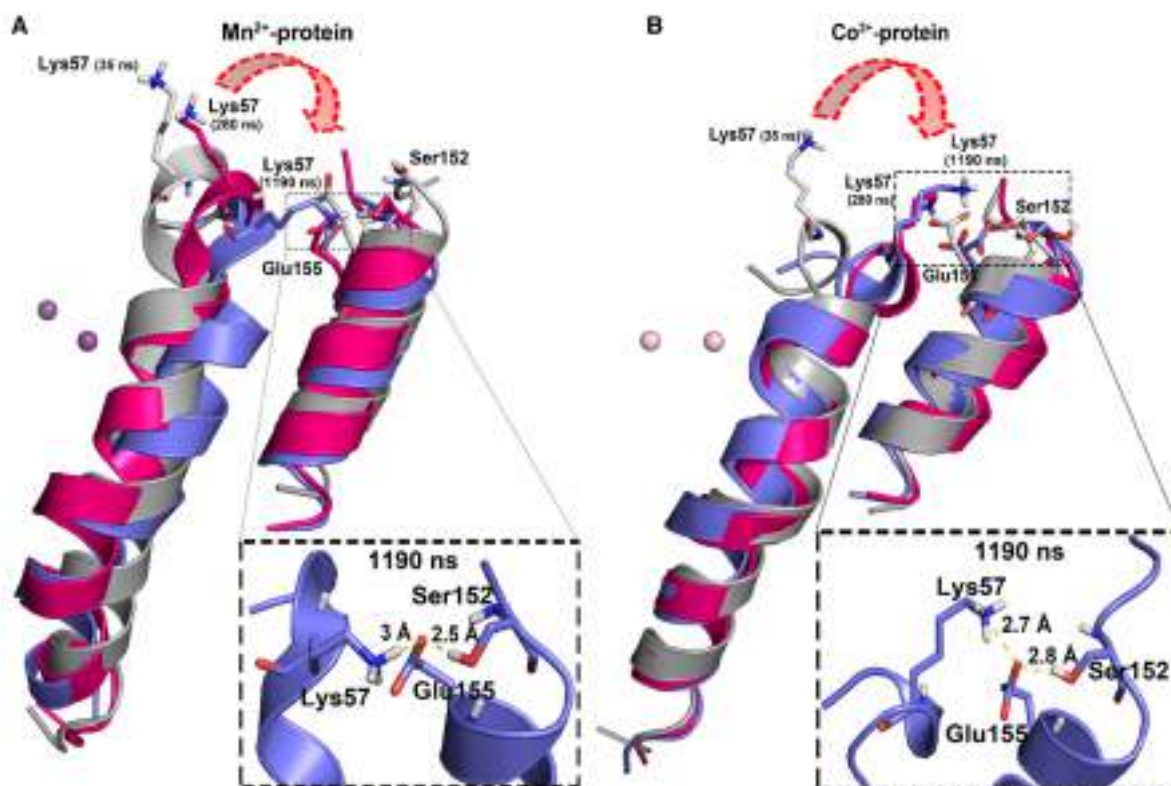


Figure 5. Interaction of Lys57-Glu155-Ser152 in *H. pylori* Mn²⁺- and Co²⁺-arginases.

The distance between the side chains of Lys57 and Glu155 decreases in (A) *H. pylori* Mn²⁺-arginase, and (B) *H. pylori* Co²⁺-arginase due to the repositioning of Lys57 as shown for the 35 (gray), 280 (pink) and 1190 ns (blue) simulated structures of the holoproteins. The position of Glu155 is relatively fixed. The enlarged figure shows the distance of Lys57–Glu155–Ser152 at 1190 ns in the holoproteins, where the interactions are mediated by the side chain of Glu155 with those of Lys57 and Ser152. The spheres represent the metal ions, Mn²⁺ (purple) and Co²⁺ (pink).

catalytic activity than the Lys57Ala variant (1.8% and 6% of wild type activity for the Lys57Arg and Lys57Ala mutants, respectively) (Table 1). The presence of a longer Arg side chain in comparison with the Lys side chain at position 57 in the Lys57Arg mutant may locally perturb the protein structure which, in turn, substantially weakens the Glu155 interactions not only with Arg57, but also with Ser152. Additionally, 3.3% of wild type activity observed in the Glu155Asp mutant may be due to the significantly weaker interactions of Asp155 with Lys57 and Ser152 in this variant with respect to those in wild type. All these results further support our observation that the interaction of Glu155 with Lys57 is crucial for catalytic function.

Table 2 Metal content in the *H. pylori* wild type and mutant Co²⁺-arginases

Protein	Number of Co ²⁺ ions per monomer
Wild type	1.9 ± 0.1
Lys57Ala	1.7 ± 0.1
Ser152Ala	1.8 ± 0.3
Lys57Ala/Ser152Ala	1.8 ± 0.2

The values represented here are the average ± SEM of three independent measurements.

We also prepared the charge reversal single (Glu155Lys and Lys57Glu) and double mutants (Lys57Glu/Glu155Lys) to further support our findings regarding the importance of the Glu155–Lys57 interaction in catalytic function. However, these three mutants could not be expressed and hence their kinetic studies were not performed. The inability to express these mutant proteins could be due to their improper folding leading to degradation.

The interactions involving Lys57–Glu155–Ser152 are extremely crucial to catalysis

As is known, an intact bimetallic centre at the active site of arginases is essential to generation of a reactive water molecule for the hydrolysis of L-arginine. To determine whether the decrease in catalytic function in the Lys57Ala, Ser152Ala, and Lys57Ala/Ser152Ala mutants was not due to the defect in the formation of a bimetallic center, the metal-binding assays were performed using reported procedures [33,43]. Similar to the wild type protein, these mutants can bridge two metal ions (Table 2). We also expressed and purified the Glu155Ala mutant using the reported procedure [39]. We performed the metal-binding assay for the Glu155Ala mutant. Similar to the previous report [39], this mutant did not exhibit detectable catalytic activity and showed the formation of an intact bimetallic centre. Additionally, the other two mutants, Glu155Asp and Lys57Arg, bridged two metal ions (data not shown). All these results indicate that the loss of catalytic function observed in the above mutants is not due to the defect in the formation of their bimetallic centre.

To determine whether the loss of catalytic activity in the three mutants (Lys57Ala, Ser152Ala, and Lys57Ala/Ser152Ala) relevant to the study of Lys57–Glu155–Ser152 interaction is due to the alteration in substrate binding, or related to a defect in catalysis, the substrate binding measurements of the wild type and mutant proteins were obtained. We used N^ω-hydroxy-L-arginine (NOHA), a known substrate analog of L-arginine for human arginase [62]. This compound has also been found to be a competitive inhibitor for the *H. pylori* enzyme. We performed intrinsic tryptophan fluorescence measurements for the wild type and mutant proteins in the presence of NOHA because the protein contains a single tryptophan near the active site. The fluorescence intensity was found to decrease with increasing concentrations of NOHA, indicating that NOHA can interact with both the wild type and mutant proteins. Figure 6A–C displays a plot of the change in fluorescence intensity with increasing concentration of NOHA. These data were fitted using a binding equation to determine the values of the dissociation constant (K_d), which were $3.3 \pm 0.5 \mu\text{M}$ for wild type, $3.8 \pm 0.6 \mu\text{M}$ for the Lys57Ala mutant and $2.8 \pm 0.1 \mu\text{M}$ for the Ser152Ala mutant. No appreciable change in the fluorescence intensity for the Lys57Ala/Ser152Ala double mutant with NOHA was observed. Hence, its K_d value could not be estimated. The insignificant change in fluorescence intensity for the double mutant in the presence of NOHA as compared with the corresponding change in the wild type may be due to a variation in tertiary structure between the wild type and double mutant. These data suggest that the mutation of Lys57, Ser152, or both to Ala did not affect the substrate binding. It may be noted that both Lys57 and Ser152 are not catalytic residues. Thus, the loss of catalytic activity is because of the defect in catalysis (see Discussion).

The interactions of Glu155 with both Lys57 and Ser152 mediate the positioning of the insertion motif

As previously described, *H. pylori* arginase is a single tryptophan protein, where Glu155 and Trp159 are located in the same insertion motif. In the *H. pylori* holoprotein, the metal-induced conformational change leads to the movement of the tryptophan into a more hydrophobic environment so that it can interact with both His122 and Tyr125. To check whether the interactions of Glu155 with both Lys57 and Ser152 have a role in the tryptophan's environment, intrinsic tryptophan fluorescence measurements of the Lys57Ala and Ser152Ala mutants were performed and the results were compared with that of wild type. Similar to the previous report, the emission maximum of the wild type holoprotein displays a blue shift of 3 nm compared with its apo-form (from 330 to 327 nm), suggesting that the microenvironment of the tryptophan appeared to be more non-polar upon binding with the metal ions (Figure 7A,B). The emission maxima of the holo-form of the Lys57Ala, Ser152Ala and Lys57Ala/Ser152Ala mutants were 328 nm (Figure 7B), indicating that the tryptophan's environment in the single and double mutant holoproteins is similar to that of wild type. These results suggest that the interactions of both Lys57 and Ser152 with Glu155 have insignificant role in the tryptophan's environment. We performed similar fluorescence measurements with the other mutant, Glu155Ala. Unlike in wild type, the fluorescence emission of the Glu155Ala mutant in the holo-form is not blue shifted compared

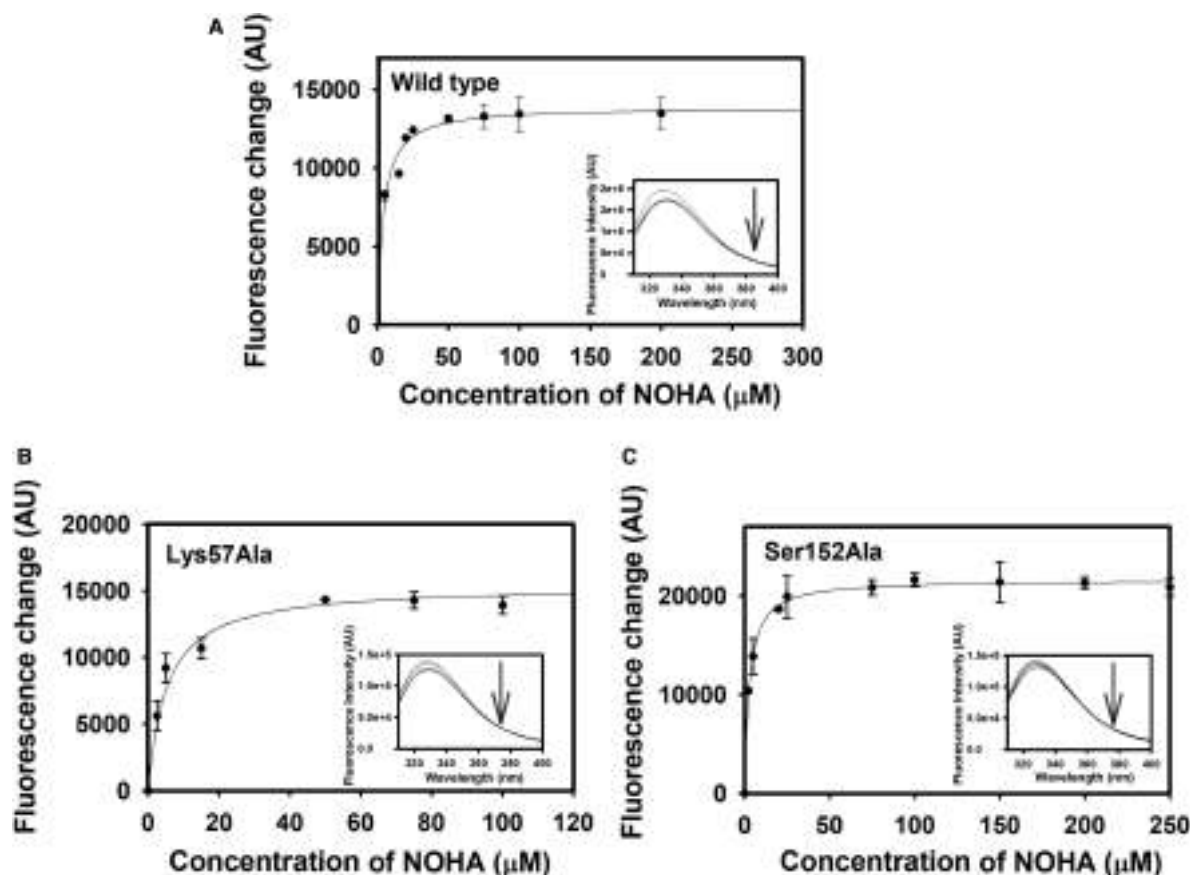


Figure 6. Measurement of the substrate binding affinity with the wild type and mutant proteins using steady-state fluorescence studies.

(A) The fluorescence intensity change of the *H. pylori* holoprotein at 327 nm with increasing concentrations of NOHA was observed upon excitation of tryptophan at 295 nm. These data were fitted to the binding equation, $\Delta F = \Delta F_{\max} \times [\text{NOHA}] / (K_d + [\text{NOHA}])$ to determine the K_d value, where ΔF is the change in fluorescence intensity. The tryptophan fluorescence intensity is found to decrease in the presence of NOHA (Inset). The protein concentration was kept at 2 μM for all experiments and the data were analyzed using the above equation. (B and C) represent similar fluorescence measurements performed for the Lys57Ala and Ser152Ala mutants, respectively. The data were analyzed as described above. In these three plots, the values represented are the average \pm SEM of three individual measurements.

with its apo-form (emission maximum ~ 330 nm) (Figure 7A,B). This suggests that the tryptophan's environment in this mutant did not change in the presence of the metal ions. The difference in the fluorescence emission maximum observed between the Glu155Ala single mutant and the Lys57Ala/Ser152Ala double mutant in their holo-form could be because of alteration in the local tertiary structure of the Glu155Ala variant.

Time-resolved fluorescence anisotropy decay measurements have been found to be very powerful in assessing the changes in the local conformation and dynamics of the protein. As already described, the indole ring of Trp159 has been shown to interact with the side chains of the non-conserved residues, His122 and Tyr125. This is suggested to be essential for positioning of the motif [40]. Glu155 is also present in the same stretch where Trp159 is located. Thus, to explore whether the interactions of Glu155 with Lys57 and Ser152 play a role in the positioning of the motif, we performed fluorescence anisotropy decay kinetic measurements using tryptophan as a probe for the wild type and mutant (Lys57Ala and Ser152Ala) holoproteins. Figure 7C shows the fluorescence decay profiles for the wild type and mutant proteins. The decay curves were fitted best to two exponential functions to determine the two rotational correlation times and their associated amplitudes. The two rotational correlation times have been interpreted as follows: The shorter rotational correlation time, ϕ_1 (corresponding amplitude, β_1), is associated with the local dynamics of the indole ring of Trp159, whereas the

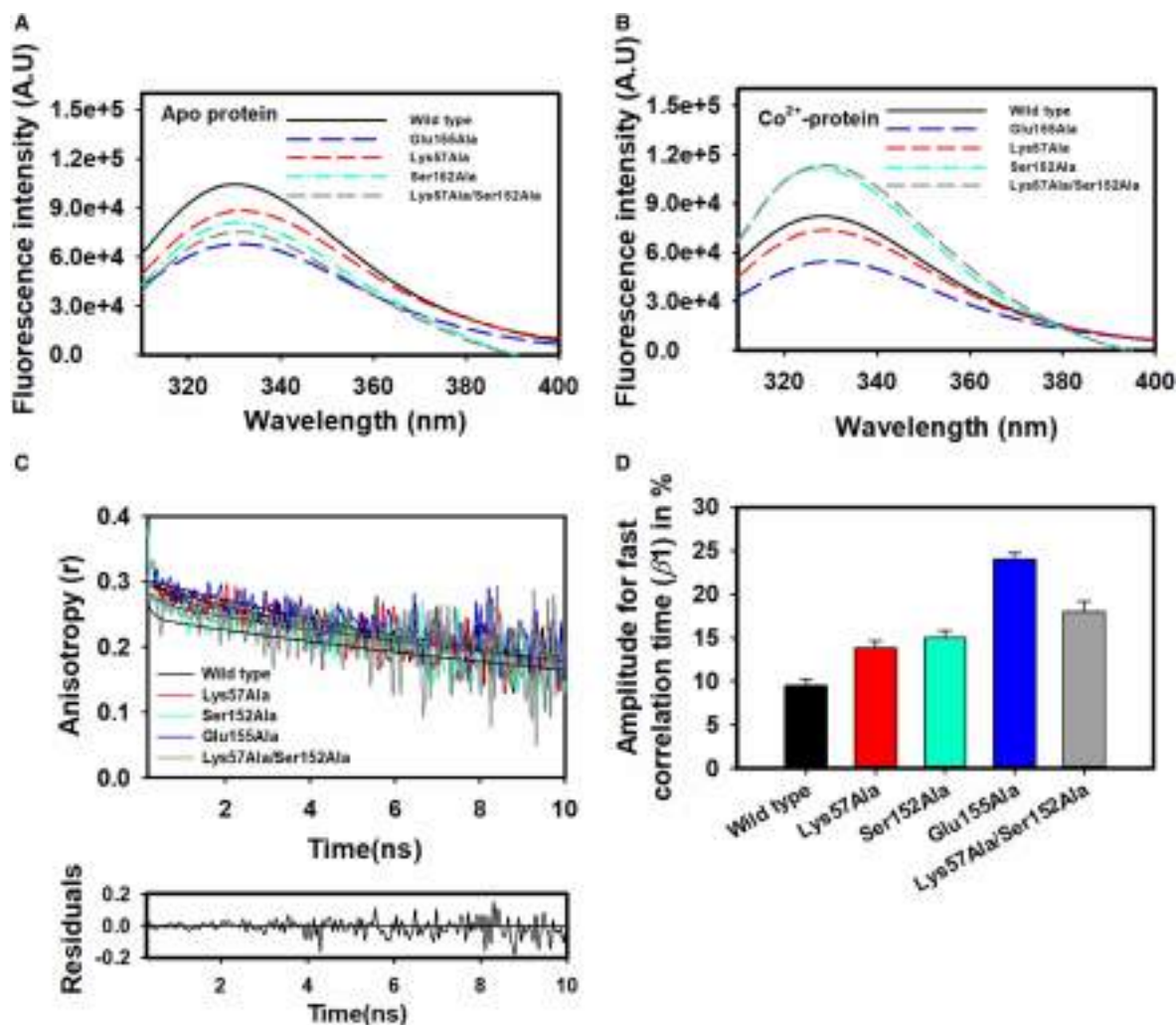


Figure 7. Tryptophan fluorescence emission spectra, and time-resolved fluorescence anisotropy decay profiles for the wild type and mutant proteins using an excitation wavelength of 295 nm.

The concentration of the protein was kept at 2 μ M. **(A)** Apoproteins and **(B)** Co²⁺-reconstituted proteins. The data represented in **A–B** are the average of three individual scans. **(C)** Time-resolved fluorescence anisotropy decay profiles for the holoproteins: wild type (black), Lys57Ala mutant (red), Ser152Ala mutant (cyan), Glu155Ala mutant (blue) and Lys57Ala/Ser152Ala double mutant (gray). The data were fitted to a two-exponential function using equation 5 shown in materials and methods. The smooth line shows a theoretical fit to the experimental data points. These profiles indicate a faster decay of fluorescence anisotropy corresponding to the shorter correlation time of Trp159 in the mutant proteins compared with that of the wild type protein. The lower panel depicts a representative random distribution showing the goodness of fit. **(D)** The amplitude β_1 associated with the shorter correlation time (ϕ_1) for the wild type and mutant protein is represented in a bar diagram. The data suggest that the indole ring of Trp159 is conformationally more flexible in the mutant proteins upon disruption of the interaction of Glu155 with Lys57, Ser152 or both. The values represented here are the average \pm SEM of three independent experiments.

longer one, ϕ_2 (corresponding amplitude, β_2), is associated with the global motion of the protein molecule. These values were extracted for the wild type and mutant proteins and are listed in Supplementary Table S2. Because the β_1 value for the wild type protein is very small (9%), the precision in the estimation of the ϕ_1 value will be less accurate. Thus, we compared the β_1 value, which would be appropriate for comparing the local dynamics of the Trp159 side chain. A lower β_1 value suggests a greater extent of the conformational rigidity and vice-versa. The observed β_1 value for the wild type protein (9%) (Figure 7D) is consistent with the

reported result [35,40] and supports the previous observation that the Trp159 side chain in the wild type holoprotein is conformationally rigid. The β_1 value for the Lys57Ala and Ser152Ala mutants was found to be 14 and 15%, respectively (Figure 7D). These results suggest that in the absence of the Lys57 or Ser152 interaction with Glu155, the rigidity of the tryptophan side chain in either of these two mutants is reduced compared with wild type. We also performed the measurement for the Glu155Ala mutant, which showed a decay profile similar to wild type. The data were similarly analyzed. The β_1 value for the Glu155Ala mutant is significantly higher compared with that of the wild type (24 versus 9% for the Glu155Ala mutant and wild type, respectively, Figure 7D). This observation suggests that the indole ring of the tryptophan in the Glu155Ala mutant is also conformationally less rigid, which may be due to the absence of the Glu155 interactions with both Lys57 and Ser152. To check this furthermore, we performed a similar measurement with the Lys57Ala/Ser152Ala double mutant, which gave a β_1 value of 18% (Figure 7D). This value was higher than that observed for the Lys57Ala or Ser152Ala mutant (14 and 15% for Lys57Ala and Ser152Ala mutants, respectively), but lower than that obtained for the Glu155Ala variant (24%). The higher β_1 value for the double mutant compared with that of their individual single mutants is likely to be because of the absence of the Glu155 interaction with either Lys57 or Ser152. The observation of a greater β_1 value for the Glu155Ala mutant than that of the Lys57Ala/Ser152Ala mutant (24 versus 18%) suggests that besides the loss of the Glu155 interactions with both Lys57 and Ser152, the mutation of Glu155 to Ala may also play a role in increasing flexibility of the tryptophan side chain. This possibly happens through a change in the orientation of the tryptophan side chain with structural change of the insertion motif upon Glu155Ala mutation. All these results indicate that the Glu155 interactions with both Lys57 and Ser152 have a role in the conformational rigidity of the Trp159 side chain and thus into the positioning of the insertion motif (see the mechanistic insight in Discussion). The fluorescence lifetime of Trp gives the value of the longer rotational correlation time, $\phi_2 > 20$ ns for the wild type holoprotein. The ϕ_2 value for the mutant holoproteins was also found to be >20 ns. However, its precise value cannot be determined.

Effect of the Lys57 or Ser152 to Ala mutation on secondary structure and stability

Our data thus far suggest that the interactions of Lys57 and Ser152 with Glu155 play an individual role in catalysis. We also wanted to understand the separate role of these two residues, Lys57 and Ser152 in secondary structure in the presence of the metal ions. To investigate this, the CD spectra of the Lys57Ala and Ser152Ala mutants in their holo-form were recorded in the far-UV range and compared with that of the wild type. The

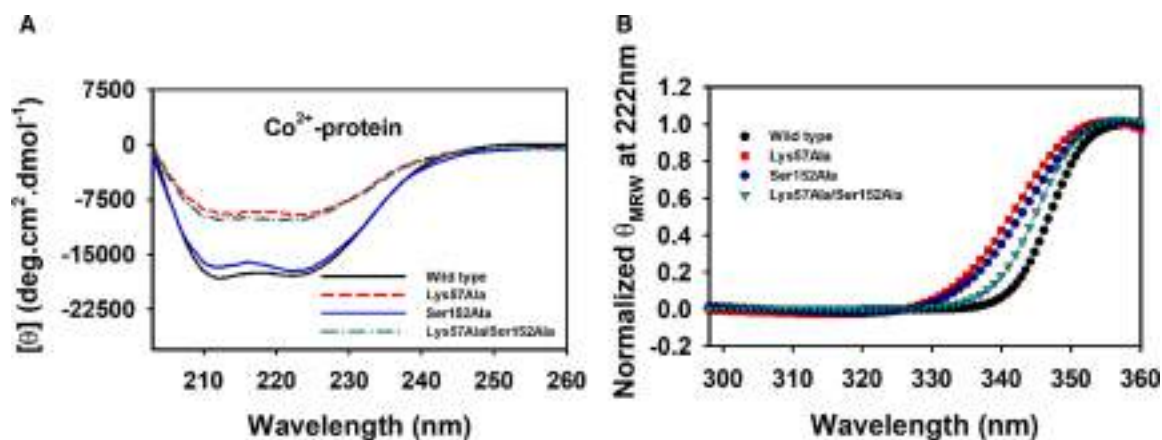


Figure 8. CD measurements of wild type and mutant proteins in the far-UV range.

(A) Circular dichroism measurements of the wild type and mutant holoproteins at pH 7.4. The data represented here are the average of three individual scans. (B) Heat-induced denaturation of the wild type and mutant Co^{2+} -reconstituted proteins determined by CD measurements at pH 7.4, 25°C. The T_m value was determined by fitting the data to a two-state unfolding curve. Three independent measurements were performed to obtain the average T_m value, but the plot shown here is a representation of one measurement.

CD intensity of the Ser152Ala mutant in the holo-form is similar to that of wild type (Figure 8A), indicating that Ser152 plays a negligible role in the secondary structure of the holoprotein. However, the CD intensity of the Lys57Ala variant was considerably lower (Figure 8A), suggesting a significant role of Lys57 in the secondary structure. We also observed a CD spectrum of the Lys57Ala/Ser152Ala mutant holoprotein similar to that of the Lys57Ala variant (Figure 8A). This supports the role of Lys57 in the secondary structure of the holoprotein. The data also suggest that the interaction of Lys57 with Glu155 may play a role in the secondary structure of the metal-reconstituted protein.

To determine whether these mutations affect stability, heat-induced denaturation studies of the wild type and mutant proteins (Lys57Ala, Ser152Ala and Lys57Ala/Ser152Ala) in their holo-form were performed using CD measurements (Figure 8B). The change in the secondary structure at 222 nm was measured with increasing temperature and their normalized $[\theta]_{MRW}$ values were plotted against the temperature. The data could be fitted to a two-state unfolding model to determine the T_m (melting temperature, a measure of thermostability). The T_m values for the wild type and mutant holoproteins were similar ($\sim 73^\circ\text{C}$, T_m values for wild type, Lys57Ala, Ser152Ala and Lys57Ala/Ser152Ala are 74 ± 0.1 , 72 ± 1.4 , 73 ± 1.2 and $73 \pm 0.3^\circ\text{C}$, respectively). This suggests that Ser152 and Lys57 individually, or together, do not play roles in providing stability to the holoprotein (see the Discussion). The data also suggest that the interaction between Lys57 and Glu155 does not play a role in determining the stability of the holoprotein. Despite a considerable decrease in the secondary structure with the mutation of Lys to Ala at position 57, the Lys57Ala and Lys57Ala/Ser152Ala variants in their holo-form showed thermal stability similar to wild type. This observation suggests that the reduced secondary structure in these two mutant proteins do not seem to play a role in stability.

As suggested, Glu155 interacts with both Lys57 and Ser152. But, the interaction with Lys57 may have a role in the secondary structure of the holoprotein. This could be because of the stronger electrostatic interaction of Glu155–Lys57 versus the weaker interaction of Glu155–Ser152. It is to be noted that the Glu155 to Ala mutation in the holoprotein was reported to show a decrease in the secondary structure similar to that of the Lys57 to Ala substitution [39]. Taken together, we suggest that the interaction of Glu155 with Lys57 plays a role in maintaining the secondary structure of the holoprotein.

Despite similar secondary structure to the wild type protein, the Ser152Ala mutant showed 74% decrease in the catalytic activity. This is likely to be because of the alteration in the local tertiary structure, which is supported by the results of the anisotropy decay kinetics of the Ser152Ala mutant. As observed, the Lys57 to Ala mutation showed 94% decrease in the catalytic activity. Thus, the additional 20% decrease in the activity observed in the Lys57Ala mutant compared with the Ser152Ala variant could be associated with a further alteration in the local tertiary structure. This may be due to the decrease in the secondary structure of the Lys57Ala mutant.

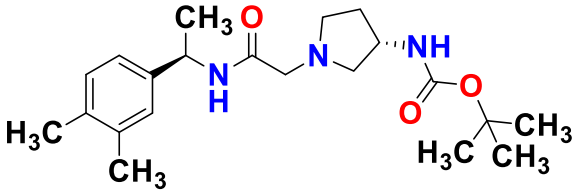
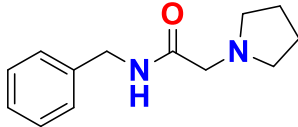
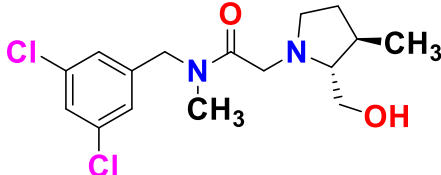
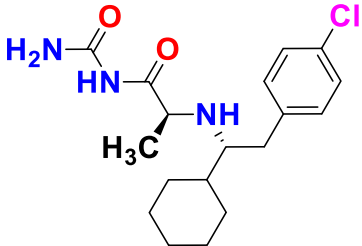
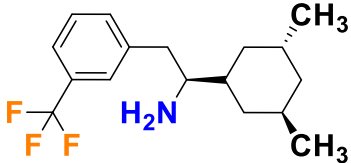
Structure-based virtual screening, molecular docking and identification of small molecule inhibitor

Our study clearly indicates that the insertion motif is critical to function through the interaction of its residue, Glu155 with both Lys57 and Ser152. Thus, this motif and its surrounding region can serve as a target site for the search of small molecule inhibitors, which could be specific to the *H. pylori* enzyme. For this purpose, we performed molecular docking based virtual screening of large dataset of small molecules with the simulated structure of the *H. pylori* holoenzyme. Molecules that bind to the above desired site with binding energy lower than -6 kcal/mol were shortlisted and further verified by AutoDock4.2. Finally, five molecules were obtained, which are listed in Table 3 and their interactions with the enzyme are shown in Supplementary Figure S2.

Enzyme inhibition assay

Out of the five shortlisted putative inhibitors, three were commercially available (named as C1, C2 and C3, Table 3) and they were tested to determine their effect on the *H. pylori* enzyme activity. The activity assay was performed individually in the presence of these three compounds using a substrate concentration, which is 4-fold greater than the K_M value of the enzyme. The rate of ornithine formation was decreased by nearly 50% in the presence of $200\ \mu\text{M}$ C3 (Figure 9A). However, the same concentration of compounds C1 and C2 showed different results; C1 increased the product formation to some extent but C2 did not display noticeable change. These results suggest that among the three compounds, C3 has an inhibitory effect on the enzyme activity. To determine the IC_{50} (half maximum inhibitory concentration) value for C3, the activity assay was further performed with varying concentrations of the inhibitor. The activity was found to decrease with

Table 3 ZINC ID and 2D structure of the five lead molecules with their binding energy obtained from molecular docking

ZINC ID (Molecular abbreviation)	Chemical structure	Binding energy (kcal/mol)
ZINC106870738 (C1)		−6.02
ZINC2860884 (C2)		−7.70
ZINC248884880 (C3)		−8.27
ZINC608981755 (C4)		−6.49
ZINC228052898 (C5)		−6.31

increasing the inhibitor concentrations, which resulted in nearly 60% maximum inhibition (Figure 9B). The IC_{50} value for C3 was found to be nearly $129 \pm 15 \mu M$, suggesting that this compound has a moderate affinity towards the *H. pylori* enzyme for the inhibition of its activity.

To examine the effect of this inhibitor on the activity of human homolog, similar activity assay measurement was performed in the presence of varying concentrations of C3. Interestingly, with this compound a marginal decrease in the product formation was observed (Figure 9C). This result suggests that the compound C3 has specificity towards the inhibition of the *H. pylori* enzyme rather than the host counterpart.

Molecular dynamics simulation studies

To understand a basis for the inhibition of the *H. pylori* enzyme activity, molecular dynamics simulations were performed for the enzyme-inhibitor complex using the lowest energy structure obtained from the molecular docking studies. The RMSD values of the enzyme-inhibitor complex varied till 100 ns, which get stabilized during the remaining simulations (Figure 9D). We also performed a clustering analysis of last 100 ns trajectory to obtain average structure of the enzyme-inhibitor complex. Figure 9E represents the average structure, which corresponds to 137 ns. Structural analysis reveals that the inhibitor interacts with the residues belonging to the non-conserved motif and other nearby regions through hydrogen bonding and hydrophobic contacts

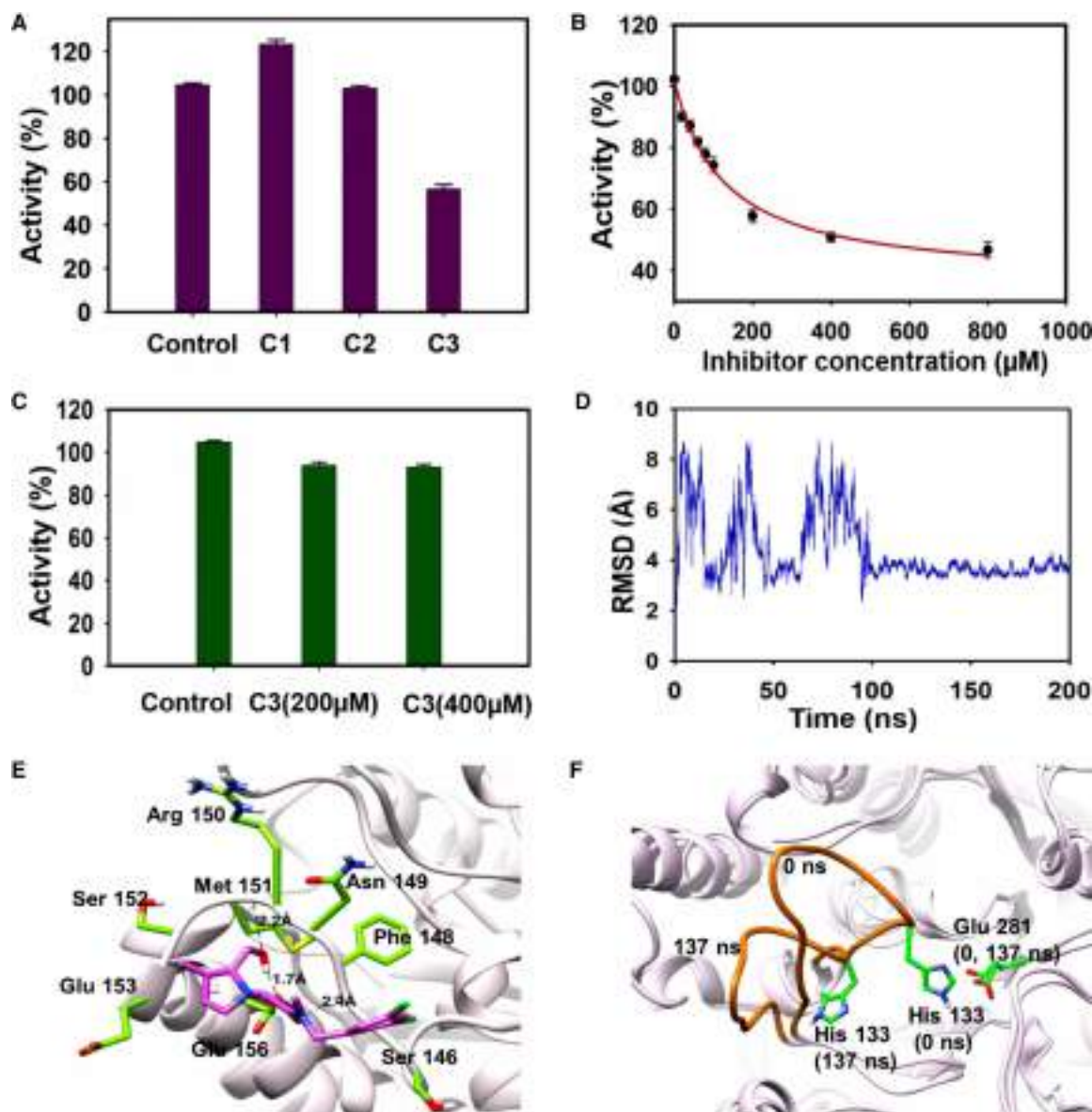


Figure 9. *In vitro* and *in silico* experiments with putative inhibitors of *H. pylori* arginase.

(A) Percentage activity of *H. pylori* Co²⁺-arginase in the presence of 200 μM of different compounds. The control indicates that the activity assay was performed in the absence of the compounds. (B) The percentage of the *H. pylori* holoenzyme activity in the presence increasing concentrations of C3 yielded the IC₅₀ value 129 ± 15 μM. (C) The percentage activity of human Co²⁺-arginase (hArg-I) in the presence of different concentrations of C3. The control indicates the enzyme activity in the absence of C3. The data shown in A–C are the average ± SEM of three individual experiments. (D) Root mean square deviation (RMSD) of *H. pylori* Co²⁺-arginase-inhibitor complex during the MD simulations. (E) Interacting residues of *H. pylori* holoarginase (green) with C3 (magenta) in the average simulated structure at 137 ns. The H-bond distances of the Glu156 side chain with -OH of C3, backbone NH of Phe148 with carbonyl oxygen of C3 and backbone NH of Met151 with hydroxyl oxygen of C3 are 1.7, 2.4 and 2.2 Å, respectively. For clarity, the remaining protein structure is omitted. (F) A change in the loop positioning containing the catalytic His133 (orange) in the simulated structure from its initial structure.

(Figure 9E). We also observed that the positioning of the loop containing the catalytic His133 in the average simulated structure is significantly varied (Figure 9F). This might explain the reduced enzyme activity observed in the presence of compound C3 (see Discussion).

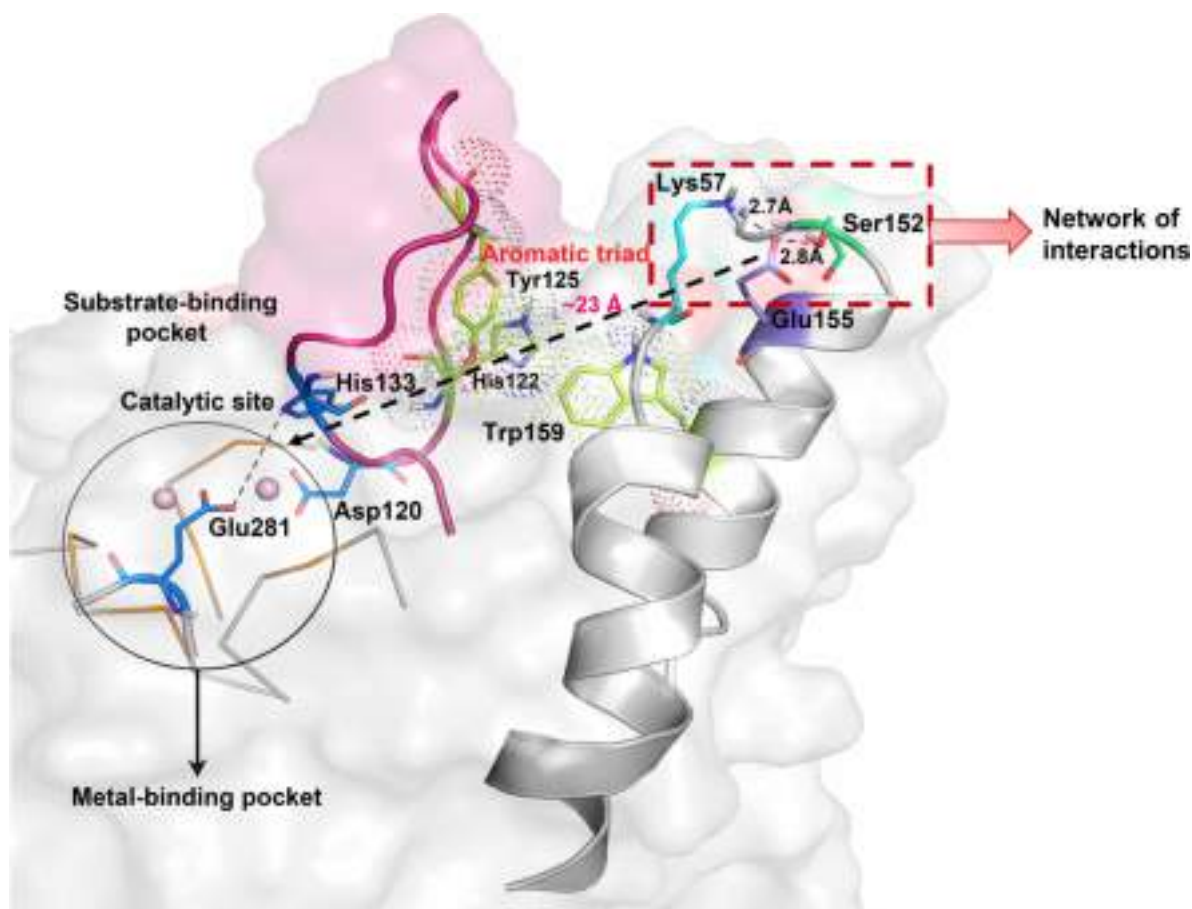


Figure 10. Schematic representation of the positioning of the insertion motif containing Glu155 through Trp159 (His122–Trp159–Tyr125) in the 1190 ns simulated structure of wild type *H. pylori* Co²⁺-arginase.

The interactions of Glu155 (purple) with Lys57 (cyan) and Ser152 (lime green) are depicted. The long-range effect of interactions involving Lys57–Glu155–Ser152 on the catalytic site (nearly 23 Å away) containing His133 and Glu281 are shown by the black dashed arrow. The loop containing the catalytic His133 is highlighted in pink and the region containing metal ion-coordinating residues (orange) is encircled.

Discussion

Arginase of *Helicobacter* gastric pathogens, including *H. pylori*, has evolved with a 13-residue-long insertion motif that is located in the middle of the protein sequence. This motif in the *H. pylori* enzyme forms a helix and is important for function and stability. However, the underlying basis for the role of this motif in terms of function has not been fully elucidated. Using *H. pylori* arginase (where *H. pylori* is known to exhibit the highest incidence of infection among *Helicobacter* gastric pathogens), the present study reveals the contact of Glu155 (belonging to this stretch) with both Lys57 and Ser152, and describes its role in the positioning of the motif. In addition, the study highlights the importance of these interactions for catalytic function through proper orientation of the loop containing the catalytic His133. Overall, these findings provide a mechanistic understanding into the role of this motif in catalysis.

How are the interactions of Glu155 with both Lys57 and Ser152 crucial to catalysis? As previously described, the structure and function of human arginase have been studied extensively. In human arginase I, the hydrolysis of L-arginine depends on the following two steps; (i) generation of a nucleophilic water molecule bridged by the two metal ions and ii) the proton transfer from a catalytic His residue to the guanidinium group of the substrate, L-arginine. The residues Glu155, Lys57, and Ser152 in the *H. pylori* enzyme are away from the catalytic loop (~23 Å from the catalytic His133 present in the same loop, Figure 10). The network of interactions

involving these three residues may have a long-range effect on either or both of these two steps through the positioning of Trp159 located in the insertion motif. It has been shown that an intact bimetallic center is essential to the generation of a nucleophilic water molecule bridged by the two metal ions. The formation of a bimetallic cluster in the Lys57Ala, Ser152Ala, and Lys57Ala/Ser152Ala mutants suggests that the interactions of Lys57, Ser152 or both with Glu155 in the wild type protein are unlikely to affect the nucleophilicity of the metal-coordinated water molecule.

The other possibility is that these interactions influence the proton transfer step. In human arginase, it has been suggested that the interaction of Glu277 with a catalytic His141 elevates the pK_a of its imidazole ring so that it remains in the protonated state at a physiological pH [21]. This is essential to the proton transfer from the catalytic His to the amino group of the intermediate species to form ornithine, an important step of L-arginine hydrolysis reaction catalyzed by arginase. Sequence comparison of *H. pylori* arginase with its human homolog reveals that the analogous residues of His141 and Glu277 in the *H. pylori* enzyme are His133 and Glu281, respectively. Structural analysis of these two homologs also reveals that the positioning of the catalytic His133 and Glu281 in *H. pylori* arginase is similar to that of their corresponding residues in the human enzyme. Moreover, it has been shown that His133 can act as a catalytic residue only when it interacts with Glu281, thereby highlighting the importance of the Glu281–His133 interaction in catalytic function [35]. It has been found that the catalytic site containing His133 and Glu281 is close to the aromatic triad, which consists of His122–Trp159–Tyr125, present exclusively in arginase of *Helicobacter* gastric pathogens. This triad is shown to be crucial to the generation of a catalytically competent conformation by maintaining the tertiary structural integrity [40]. Moreover, the two residues His122 and Tyr125 of the triad are present in a loop, which consists of 13-residues ($-^{122}\text{HTAYDSDSKHIHG}^{134}-$) (Figure 10). Interestingly, this loop contains the catalytic His133. Therefore, it appears that the interactions of His122 and Tyr125 with Trp159, through their side chains, position the loop in such a way that His133 becomes closer to Glu281. It may be noted that, in other bacterial and human homologs, the above analogous loop region of *H. pylori* arginase forms a loop-cum-helix, where the catalytic His is present in a helix [35]. Thus, the positioning of this His is likely to be fixed and nearer to the Glu residue. The presence of the catalytic His in a loop of the *H. pylori* enzyme is perhaps the reason why the protein has evolved with both His122 and Tyr125 along with Trp159 to properly position His133 for catalytic function.

As observed in this study, Glu155 plays a role in the positioning of the insertion motif mediated by Trp159. To determine whether the Lys57–Glu155–Ser152 interactions can affect the Glu281–His133 contact and thus the proton transfer, we created three *in silico* point mutants (Lys57Ala, Ser152Ala and Glu155Ala) using the simulated structure of *H. pylori* Co^{2+} -arginase and performed their MD simulation studies until 100 ns, where equilibrium structures were obtained (Supplementary Figure S3). We analyzed their individual structures and estimated the distance between Glu281 and His133 (Supplementary Figure S4). This was found to be 9.8, 9.6 and 6.7 Å for the Glu155Ala, Lys57Ala and Ser152Ala mutants, respectively, which was higher than that of the wild type (5 Å). These results suggest that the individual mutation of three residues affects the distance between Glu281 and His133 in the following order: Glu155Ala > Lys57Ala > Ser152Ala. We also compared the positioning of Glu281 and His133 in the mutant proteins versus the wild type (Supplementary Figure S5). We observed that the positioning of Glu281 in the mutants is similar. However, the positioning of His133 is changed. This could be because of the variation in the orientation of the loop containing this residue. It was previously reported that, in solution, the distance between His133 and Glu281 of the wild type holoprotein is suggested to decrease upon heat activation through a metal-induced conformational rearrangement near the active site so that the proton transfer can occur from the catalytic His133 [35]. In general, the preparation of holoarginases with heat activation is essential to higher catalytic activity. It has been shown that the *H. pylori* holoenzyme with heat activation exhibits higher catalytic activity compared with that without heat activation [8,33]. Thus, in solution, the observed distance between Glu281 and His133 in the mutant holoproteins might decrease upon heat activation, but their proximity will not be adequate for efficient proton transfer. This might lead to significantly reduced catalytic activity. Thus, these results seem to provide new insight into the effect of the Lys57–Glu155–Ser152 interactions on the positioning of the loop containing the catalytic His133 through Trp159 of the insertion motif so that His133 is nearer to Glu281 for efficient catalysis.

What may be the reason for the reduced enzyme activity in the presence of compound C3? As observed, the positioning of the loop containing the catalytic His133 is changed in the presence of the inhibitor (Figure 9F). The inhibitor is found to interact with Glu156, which is adjacent to Glu155 and also part of the insertion motif (Figure 9E). As previously discussed, the Glu281–His133 interaction is mediated by Glu155. Since the proper

orientation of the loop containing His133 is essential for its interaction with Glu281, the variation in the loop positioning with the inhibitor resulted in an apparent increase in the distance between His133 and Glu281, thereby possibly affecting the catalysis. It may be noted that throughout the simulations with the inhibitor the positioning of Glu281 is almost unaffected (Figure 9F).

As previously described, the insertion motif is found only in the arginase of *Helicobacter* gastric pathogens, where Glu155 is strictly conserved. It is interesting to note that Lys57 is also observed only in the arginase of these pathogens (Figure 1). These observations suggest that the two oppositely charged residues, Lys57 and Glu155, of arginase in *Helicobacter* gastric pathogens might have been selected during the evolution of this enzyme to maintain a catalytically competent conformation, possibly through the formation of required secondary structure. However, an Asn is found instead of a Ser at the analogous position of 152 in the arginase of other *Helicobacter* gastric pathogens, which may play a similar role in the function (Figure 1). This may explain the greater role of Lys57 compared with Ser152 in the catalytic function of *H. pylori* arginase.

In conclusion, this study identifies two non-catalytic residues, Lys57 and Ser152, in *H. pylori* holoarginase, whose interactions with Glu155 (electrostatic and H-bonding, respectively) are essential to the positioning of the insertion motif through Trp159 located near the active site. This generates a conformation that is catalytically competent for the hydrolytic reaction of L-arginine through the proper orientation of the loop containing His133, which can bring this His nearer to Glu281 for catalysis. Effect of such interactions on catalysis in the *H. pylori* enzyme seems to be novel among arginases. This may be important for the pathogenesis of the bacterium in the human stomach. Thus, the study highlights the importance of a network of interactions involving a unique set of residues (Lys57 and Glu155) for catalysis. Although the study identifies a new inhibitor with moderate affinity specific to the *H. pylori* enzyme, there is a scope to design inhibitors with greater affinity and higher efficacy on the basis of the molecular architecture of compound C3, which is currently underway.

Data Availability

All data generated during this study are included in this article and its supporting information file.

Competing Interests

The authors declare that there are no competing interests associated with the manuscript.

Funding

A.D. thanks the Council of Scientific and Industrial Research, India for granting research fellowship. P. M. thanks Department of Biotechnology, India for providing the fellowship of Research Associate position. This work was funded by the National Institute of Immunology, New Delhi and Department of Biotechnology [BT/PR22909/MED/29/1177/2016], India.

CRedit Contribution

Apurba Kumar Sau: Conceptualization, Resources, Supervision, Funding acquisition, Validation, Writing — original draft, Project administration, Writing — review and editing. **Ankita Dutta:** Conceptualization, Validation, Investigation, Writing — original draft, Writing — review and editing. **Ditsa Sarkar:** Validation, Investigation, Writing — review and editing. **Pooja Murarka:** Validation, Investigation, Writing — review and editing. **Tasneem Kausar:** Investigation, Visualization, Writing — review and editing. **Satya Narayan:** Data curation, Formal analysis. **Mohit Mazumder:** Data curation, Investigation, Writing — review and editing. **Sri Rama Koti Ainavarapu:** Formal analysis. **Samudrala Gourinath:** Formal analysis.

Acknowledgements

We thank Dr. N. Periasamy for the software used in the analysis of time-resolved fluorescence data. We thank the advanced instrumentation research facility of Jawaharlal Nehru University (JNU) for providing access to perform circular dichroism measurements.

Abbreviations

CD, circular dichroism; IRF, instrument response factor; MD, molecular dynamics; NO, nitric oxide; NOHA, N^ω-hydroxy-L-arginine; RMSD, root-mean-square deviation.

References

- Conteduca, V., Sansonno, D., Lauletta, G., Russi, S., Ingravalle, G. and Dammacco, F. (2013) *H. pylori* infection and gastric cancer: State of the art (Review). *Int. J. Oncol.* **42**, 5–18 <https://doi.org/10.3892/ijo.2012.1701>
- Marshall, B.J. and Warren, J.R. (1984) Unidentified curved bacilli in the stomach of patients with gastritis and peptic ulceration. *Lancet* **323**, 1311–1315 [https://doi.org/10.1016/S0140-6736\(84\)91816-6](https://doi.org/10.1016/S0140-6736(84)91816-6)
- Ye, W., Held, M., Lagergren, J., Engstrand, L., Blot, W.J., McLaughlin, J.K. et al. (2004) *Helicobacter pylori* infection and gastric atrophy: risk of adenocarcinoma and squamous-cell carcinoma of the esophagus and adenocarcinoma of the gastric cardia. *J. Natl. Cancer Inst.* **96**, 388–396 <https://doi.org/10.1093/jnci/djh057>
- Uemura, N., Okamoto, S., Yamamoto, S., Matsumura, N., Yamaguchi, S., Yamakido, M. et al. (2001) *Helicobacter pylori* infection and the development of gastric cancer. *N. Engl. J. Med.* **345**, 784–789 <https://doi.org/10.1056/NEJMoa001999>
- Correa, P. (1992) Human gastric carcinogenesis: a multistep and multifactorial process- first American cancer society award lecture on cancer epidemiology and prevention. *Cancer Res.* **52**, 6735–6740 PMID:1458460
- Srivastava, A., Dwivedi, N. and Sau, A.K. (2010) Role of a disulphide bond in *Helicobacter pylori* arginase. *Biochem. Biophys. Res. Commun.* **395**, 348–351 <https://doi.org/10.1016/j.bbrc.2010.04.014>
- Mendz, G.L., Holmes, E.M. and Ferrero, R.L. (1998) In situ characterization of *Helicobacter pylori* arginase. *Biochim. Biophys. Acta Protein Struct. Mol. Enzymol.* **1388**, 465–477 [https://doi.org/10.1016/S0167-4838\(98\)00207-6](https://doi.org/10.1016/S0167-4838(98)00207-6)
- McGee, D.J., Zabaleta, J., Viator, R.J., Testerman, T.L., Ochoa, A.C. and Mendz, G.L. (2004) Purification and characterization of *Helicobacter pylori* arginase, RocF: Unique features among the arginase superfamily. *Eur. J. Biochem.* **271**, 1952–1962 <https://doi.org/10.1111/j.1432-1033.2004.04105.x>
- McGee, D.J., Radcliff, F.J., Mendz, G.L., Ferrero, R.L. and Mobley, H.L.T. (1999) *Helicobacter pylori* rocF is required for arginase activity and acid protection in vitro but is not essential for colonization of mice or for urease activity. *J. Bacteriol.* **181**, 7314–7322 <https://doi.org/10.1128/JB.181.23.7314-7322.1999>
- Hovey, J.G., Watson, E.L., Langford, M.L., Hildebrandt, E., Bathala, S., Bolland, J.R. et al. (2007) Genetic microheterogeneity and phenotypic variation of *Helicobacter pylori* arginase in clinical isolates. *BMC Microbiol.* **7**, 1–15 <https://doi.org/10.1186/1471-2180-7-26>
- Gobert, A.P., Cheng, Y., Wang, J.-Y., Boucher, J.-L., Iyer, R.K., Cederbaum, S.D. et al. (2002) *Helicobacter pylori* induces macrophage apoptosis by activation of arginase II. *J. Immunol.* **168**, 4692–4700 <https://doi.org/10.4049/jimmunol.168.9.4692>
- Fu, S., Ramanujam, K.S., Wong, A., Fantry, G.T., Drachenberg, C.B., James, S.P. et al. (1999) Increased expression and cellular localization of inducible nitric oxide synthase and cyclooxygenase 2 in *Helicobacter pylori* gastritis. *Gastroenterology* **116**, 1319–1329 [https://doi.org/10.1016/S0016-5085\(99\)70496-8](https://doi.org/10.1016/S0016-5085(99)70496-8)
- Bussière, F.I., Chaturvedi, R., Cheng, Y., Gobert, A.P., Asim, M., Blumberg, D.R., et al. (2005) Spermine causes loss of innate immune response to *Helicobacter pylori* by inhibition of inducible nitric-oxide synthase translation. *J. Biol. Chem.* **280**, 2409–2412 <https://doi.org/10.1074/jbc.C400498200>
- Zabaleta, J., McGee, D.J., Zea, A.H., Hernández, P., Rodríguez, P.C., Sierra, R.A. et al. (2004) *Helicobacter pylori* arginase inhibits T cell proliferation and reduces the expression of the TCR ζ -Chain (CD3 ζ). *J. Immunol.* **173**, 586–593 <https://doi.org/10.4049/jimmunol.173.1.586>
- Nathan, C. and Shiloh, M.U. (2000) Reactive oxygen and nitrogen intermediates in the relationship between mammalian hosts and microbial pathogens. *Proc. Natl Acad. Sci. U.S.A.* **97**, 8841–8848 <https://doi.org/10.1073/pnas.97.16.8841>
- Gobert, A.P., McGee, D.J., Akhtar, M., Mendz, G.L., Newton, J.C., Cheng, Y. et al. (2001) *Helicobacter pylori* arginase inhibits nitric oxide production by eukaryotic cells: A strategy for bacterial survival. *Proc. Natl Acad. Sci. U.S.A.* **98**, 13844–13849 <https://doi.org/10.1073/pnas.241443798>
- Baldari, C.T., Lanzavecchia, A. and Telford, J.L. (2005) Immune subversion by *Helicobacter pylori*. *Trends Immunol.* **26**, 199–207 <https://doi.org/10.1016/j.it.2005.01.007>
- Carvajal, N., Venegas, A., Oestreicher, G. and Plaza, M. (1971) Effect of manganese on the quaternary structure of human liver arginase. *Biochim. Biophys. Acta Enzymol.* **250**, 437–442 [https://doi.org/10.1016/0005-2744\(71\)90200-2](https://doi.org/10.1016/0005-2744(71)90200-2)
- Carvajal, N., Lopez, V., Uribe, E., Herrera, P. and Cerpa, J. (1999) Manganese-dependent inhibition of human liver arginase by borate. *J. Inorg. Biochem.* **77**, 163–167 [https://doi.org/10.1016/S0162-0134\(99\)00187-7](https://doi.org/10.1016/S0162-0134(99)00187-7)
- Grobbe, Y., Uitdehaag, J.C.M., Willemsen-Seegers, N., Tabak, W.W.A., de Man, J., Buijsman, R.C. et al. (2020) Structural insights into human arginase-1 pH dependence and its inhibition by the small molecule inhibitor CB-1158. *J. Struct. Biol.* **4**, 100014 <https://doi.org/10.1016/j.jsbx.2019.100014>
- Di Costanzo, L., Sabio, G., Mora, A., Rodríguez, P.C., Ochoa, A.C., Centeno, F. et al. (2005) Crystal structure of human arginase I at 1.29-Å resolution and exploration of inhibition in the immune response. *Proc. Natl Acad. Sci. U.S.A.* **102**, 13058–13063 <https://doi.org/10.1073/pnas.0504027102>
- Zakharin, T.Y., Di Costanzo, L., Christianson, D.W. and Pennsly, V. (2008) (S)-2-Amino-6-nitrohexanoic acid binds to human arginase I through multiple nitro-metal coordination interactions in the binuclear manganese cluster. *J. Am. Chem. Soc.* **130**, 17254–17255 <https://doi.org/10.1021/ja807702q>
- Stone, E.M., Chantranupong, L. and Georgiou, G. (2010) The second-shell metal ligands of human arginase affect coordination of the nucleophile and substrate. *Biochemistry* **49**, 10582–10588 <https://doi.org/10.1021/bi101542t>
- Cama, E., Colletuori, D.M., Emig, F.A., Shin, H., Kim, S.W., Kim, N.N. et al. (2003) Human arginase II: crystal structure and physiological role in male and female sexual arousal. *Biochemistry* **42**, 8445–8451 <https://doi.org/10.1021/bi034340j>
- Colletuori, D.M. and Ash, D.E. (2001) Classical and slow-binding inhibitors of human type II arginase. *Biochemistry* **40**, 9356–9362 <https://doi.org/10.1021/bi010783g>
- Antonio, E.L.D., Hai, Y. and Christianson, D.W. (2012) Structure and function of non-native metal clusters in human arginase. *Biochemistry* **51**, 8399–8409 <https://doi.org/10.1021/bi301145n>
- Sadarangani, V., Rahman, S. and Sau, A.K. (2018) Metal ions-induced stability and function of bimetallic human arginase-I, a therapeutically important enzyme. *Biochim. Biophys. Acta Proteins Proteomics* **1866**, 1153–1164 <https://doi.org/10.1016/j.bbapap.2018.08.006>
- Di Costanzo, L., Ilies, M., Thorn, K.J. and Christianson, D.W. (2010) Inhibition of human arginase I by substrate and product analogues. *Arch. Biochem. Biophys.* **496**, 101–108 <https://doi.org/10.1016/j.abb.2010.02.004>
- Bewley, M.C., Jeffrey, P.D., Patchett, M.L., Kanyo, Z.F. and Baker, E.N. (1999) Crystal structures of *Bacillus caldovelox* arginase in complex with substrate and inhibitors reveal new insights into activation, inhibition and catalysis in the arginase superfamily. *Structure* **7**, 435–448 [https://doi.org/10.1016/S0969-2126\(99\)80056-2](https://doi.org/10.1016/S0969-2126(99)80056-2)
- Müller, I.B., Walter, R.D. and Wrenger, C. (2005) Structural metal dependency of the arginase from the human malaria parasite *Plasmodium falciparum*. *Biol. Chem.* **386**, 117–126 <https://doi.org/10.1515/BC.2005.015>

- 31 Christianson, D.W. and Cox, J.D. (1999) Catalysis By metal-Activated hydroxide in zinc and manganese metalloenzymes. *Annu. Rev. Biochem.* **68**, 33–57 <https://doi.org/10.1146/annurev.biochem.68.1.33>
- 32 Carvajal, N., Acoria, M., Rodríguez, J.P., Fernández, M. and Martínez, J. (1982) Evidence for cooperative effects in human liver arginase. *Biochim. Biophys. Acta Protein Struct. Mol. Enzymol.* **701**, 146–148 [https://doi.org/10.1016/0167-4838\(82\)90324-7](https://doi.org/10.1016/0167-4838(82)90324-7)
- 33 Srivastava, A. and Sau, A.K. (2010) Biochemical studies on *Helicobacter pylori* arginase: Insight into the difference in activity compared to other arginases. *IUBMB Life* **62**, 906–915 <https://doi.org/10.1002/iub.401>
- 34 Zhang, X., Zhang, J., Zhang, R., Guo, Y., Wu, C., Mao, X. et al. (2013) Structural, enzymatic and biochemical studies on *Helicobacter pylori* arginase. *Int. J. Biochem. Cell Biol.* **45**, 995–1002 <https://doi.org/10.1016/j.biocel.2013.02.008>
- 35 Dutta, A., Mazumder, M., Alam, M., Gourinath, S. and Sau, A.K. (2019) Metal-induced change in catalytic loop positioning in *Helicobacter pylori* arginase alters catalytic function. *Biochem. J.* **476**, 3595–3614 <https://doi.org/10.1042/BCJ20190545>
- 36 García, D., Uribe, E., Lobos, M., Orellana, M.S. and Carvajal, N. (2009) Studies on the functional significance of a C-terminal S-shaped motif in human arginase type I: Essentiality for cooperative effects. *Arch. Biochem. Biophys.* **481**, 16–20 <https://doi.org/10.1016/j.abb.2008.10.015>
- 37 Marino, T., Russo, N. and Toscano, M. (2013) What occurs by replacing Mn²⁺ with Co²⁺ in human arginase I: First-principles computational analysis. *Inorg. Chem.* **52**, 655–659 <https://doi.org/10.1021/ic301703t>
- 38 Stone, E.M., Glazer, E.S., Chanturanpong, L., Cherukuri, P., Breece, R.M., Tierney, D.L. et al. (2010) Replacing Mn²⁺ with Co²⁺ in human arginase I enhances cytotoxicity towards L-arginine auxotrophic cancer cell lines. *ACS Chem. Biol.* **5**, 333–342 <https://doi.org/10.1021/cb900267j>
- 39 Srivastava, A., Meena, S.K., Alam, M., Nayeem, S.M., Deep, S. and Sau, A.K. (2013) Structural and functional insights into the regulation of *Helicobacter pylori* arginase activity by an evolutionary nonconserved motif. *Biochemistry* **52**, 508–519 <https://doi.org/10.1021/bi301421v>
- 40 George, G., Kombrabail, M., Ranninga, N. and Sau, A.K. (2017) Arginase of helicobacter gastric pathogens uses a unique set of non-catalytic residues for catalysis. *Biophys. J.* **112**, 1120–1134 <https://doi.org/10.1016/j.bpj.2017.02.009>
- 41 Solnick, J.V. and Schauer, D.B. (2001) Emergence of diverse *Helicobacter* species in the pathogenesis of gastric and enterohepatic diseases. *Clin. Microbiol. Rev.* **14**, 59–97 <https://doi.org/10.1128/CMR.14.1.59-97.2001>
- 42 Purbey, P.K., Jayakumar, P.C., Patole, M.S. and Galande, S. (2006) pC6-2/caspase-6 system to purify glutathione-S-transferase-free recombinant fusion proteins expressed in *Escherichia coli*. *Nat. Protoc.* **1**, 1820–1827 <https://doi.org/10.1038/nprot.2006.310>
- 43 Ahrland, S. and Herman, R.G. (1975) Spectrophotometric determination of manganese(II) and zinc(II) with 4-(2-pyridylazo)resorcinol (PAR). *Anal. Chem.* **47**, 2422–2426 <https://doi.org/10.1021/ac60364a028>
- 44 Mukhopadhyay, S., Nayak, P.K., Udgaonkar, J.B. and Krishnamoorthy, G. (2006) Characterization of the formation of amyloid protofibrils from barstar by mapping residue-specific fluorescence dynamics. *J. Mol. Biol.* **358**, 935–942 <https://doi.org/10.1016/j.jmb.2006.02.006>
- 45 Jha, A., Ishii, K., Udgaonkar, J.B., Tahara, T. and Krishnamoorthy, G. (2011) Exploration of the correlation between solvation dynamics and internal dynamics of a protein. *Biochemistry* **50**, 397–408 <https://doi.org/10.1021/bi101440c>
- 46 Bevington, P.R. (1969) *Data Reduction and Error Analysis for the Physical Sciences*, McGraw-Hill, New York, NY
- 47 Morris, G.M., Huey, R., Lindstrom, W., Sanner, M.F., Bellew, R.K., Goodsell, D.S. et al. (2009) Autodock4 and AutoDockTools4: automated docking with selective receptor flexibility. *J. Comput. Chem.* **30**, 2785–2791 <https://doi.org/10.1002/jcc.21256>
- 48 Dallakyan, S. and Olson, A.J. (2015) Small-molecule library screening by docking with PyRx. *Methods Mol. Biol.* **1263**, 243–250 https://doi.org/10.1007/978-1-4939-2269-7_19
- 49 Trott, O. and Olson, A.J. (2010) Autodock Vina: improving the speed and accuracy of docking with a new scoring function, efficient optimization, and multithreading. *J. Comput. Chem.* **31**, 455–461 <https://doi.org/10.1002/jcc.21334>
- 50 Lauck, F., Smith, C.A., Friedland, G.F., Humphris, E.L. and Kortemme, T. (2010) RosettaBackrub—a web server for flexible backbone protein structure modeling and design. *Nucleic Acids Res.* **38**, W569–W575 <https://doi.org/10.1093/nar/gkq369>
- 51 Case, D.A., Walker, R.C., Cheatham, III, T.E., Simmerling, C., Roitberg, A., Merz, K.M. et al. Amber 12 Reference Manual Principal contributors to the current codes
- 52 Delano, W.L. PyMOL: An Open-Source Molecular Graphics Tool
- 53 Salomon-Ferrer, R., Götz, A.W., Poole, D., Le Grand, S. and Walker, R.C. (2013) Routine microsecond molecular dynamics simulations with AMBER on GPUs. 2. Explicit solvent particle mesh ewald. *J. Chem. Theory Comput.* **9**, 3878–3888 <https://doi.org/10.1021/ct400314y>
- 54 Abraham, M.J., Murtola, T., Schulz, R., Páll, S., Smith, J.C., Hess, B. et al. (2015) GROMACS: High performance molecular simulations through multi-level parallelism from laptops to supercomputers. *SoftwareX* **1–2**, 19–25 <https://doi.org/10.1016/j.softx.2015.06.001>
- 55 Van Der Spoel, D., Lindahl, E., Hess, B., Groenhof, G., Mark, A.E. and Berendsen, H.J.C. (2005) GROMACS: fast, flexible, and free. *J. Comput. Chem.* **26**, 1701–1718 <https://doi.org/10.1002/jcc.20291>
- 56 Wang, J., Wolf, R.M., Caldwell, J.W., Kollman, P.A. and Case, D.A. (2004) Development and testing of a general amber force field. *J. Comput. Chem.* **25**, 1157–1174 <https://doi.org/10.1002/jcc.20035>
- 57 Jakalian, A., Jack, D.B. and Bayly, C.I. (2002) Fast, efficient generation of high-quality atomic charges. AM1-BCC model: II. Parameterization and validation. *J. Comput. Chem.* **23**, 1623–1641 <https://doi.org/10.1002/jcc.10128>
- 58 Case, D.A., Ben-Shalom, I.Y., Brozell, S.R., Cerutti, D.S., Cheatham, III, T.E., Cruzeiro, V.W.D. et al. (2018) *Amber 2018 Reference Manual*, University of California, San Francisco
- 59 Lindorff-Larsen, K., Piana, S., Palmo, K., Maragakis, P., Klepeis, J.L., Dror, R.O. et al. (2010) Improved side-chain torsion potentials for the Amber ff99SB protein force field. *Proteins* **78**, 1950–1958 <https://doi.org/10.1002/prot.22711>
- 60 Kausar, T. and Nayeem, S. (2018) Identification of small molecule inhibitors of ALK2: a virtual screening, density functional theory, and molecular dynamics simulations study. *J. Mol. Model.* **24**, 261 <https://doi.org/10.1007/s00894-018-3789-2>
- 61 Srivastava, A., Dwivedi, N., Samanta, U. and Sau, A.K. (2011) Insight into the role of a unique SSEHA motif in the activity and stability of *Helicobacter pylori* arginase. *IUBMB Life* **63**, 1027–1036 <https://doi.org/10.1002/iub.552>
- 62 Boucher, J.L., Custot, J., Vadon, S., Delaforge, M., Lepoivre, M., Tenu, J.P. et al. (1994) N ω -hydroxy-L-arginine, an intermediate in the L-arginine to nitric oxide pathway, is a strong inhibitor of liver and macrophage arginase. *Biochem. Biophys. Res. Commun.* **203**, 1614–1621 <https://doi.org/10.1006/bbrc.1994.2371>